New tools for network time series with an application to COVID-19 hospitalisations

G. P. Nason*†, D. Salnikov*†
Imperial College London
and
M. Cortina–Borja†*
Great Ormond Street Institute of Child Health
University College London

April 7, 2025

Abstract

Network time series models are increasingly important across many areas, involving known or inferred underlying network structure, which can be exploited to make sense of high–dimensional dynamic phenomena. We introduce two new association measures: the network and partial network autocorrelation functions and define Corbit (correlation–orbit) visualisation plots. Corbit plots permit interpretation of underlying correlation structures and, crucially, aid model selection more rapidly than general tools such as information criteria. We introduce interpretations of generalised network autoregressive (GNAR) processes as generalised graphical models. We shine new light on how incorporating prior information is related to variable selection and shrinkage in the GNAR context. We illustrate the usefulness of GNAR models, network autocorrelations and Corbit plots for a novel network time series modelling of COVID–19 mechanical ventilation bed occupancies at 140 NHS Trusts. We also introduce the R–Corbit plot that shows correlations over different time periods or with respect to external covariates and plots that quantify the relevance of individual nodes. Our analysis provides insight on the COVID–19 series' underlying dynamics, highlights two groups of geographically co–located 'relevant' NHS Trusts, and demonstrates excellent predictive performance.

Keywords: multivariate time series, network autocorrelation function, partial network autocorrelation function, Corbit plot, R–Corbit plot.

*Dept. Mathematics, Huxley Building, Imperial College, 180 Queen's Gate, South Kensington, London, SW7 2AZ, UK.

†Population, Policy and Practice Research and Teaching Department, Great Ormond Street Institute of Child Health, 30 Guilford Street, London, WC1N 1EH, UK.

1 Introduction

Network time series in many areas benefit from the development of statistical methods that enable interpretation and inference of relationships present in dynamic phenomena. Modelling such network time series necessitates studying a constant flux of complex data characterised by a temporal component among large numbers of interacting variables. The interacting variables are often associated with a network structure, for example, networks in neuroscience, biology, medicine and business to name a few. In the absence of a network, techniques are available to learn possible network structure, which enables efficient modelling, analysis and forecasting of a large number of interactions; see, e.g., Lauritzen (2004); Friedman et al. (2008); Songsiri et al. (2009). A complete overview of network science and multivariate time series is beyond the scope of this work; see Silva et al. (2021) for a review. For a non-exhaustive overview of network methods in statistics *and* time series see, e.g., Dahlhaus (2000); Lauritzen (2004); Lütkepohl (2005); Brockwell and Davis (2006); Songsiri et al. (2009); Kolaczyk (2009); Shumway (2017) and Dallakyan et al. (2022).

Recently, the generalized network autoregressive (GNAR) model has been developed (Knight et al., 2016; Zhu et al., 2017; Knight et al., 2020), which provides a parsimonious interpretable model that has been often shown to have both simpler interpretability *and* superior forecasting performance in a number of scenarios. Model extensions in this rapidly developing area include, for example, Zhu et al. (2019) for quantiles, Zhou et al. (2020) for Network GARCH models, Nason and Wei (2022) to admit time-changing exogeneous variables, Armillotta and Fokianos (2021, 2024) for Poisson/count data, Mantziou et al. (2023) for GNAR processes on the edges of networks, and Yin et al. (2023) develop a model with local per–node network parameters along with a test for equality and subsequent asymptotic theory. Such models have proven useful for many (network) time series where the characteristics of the series are similar from variable (node) to variable (node) in a network, although GNAR processes' utility is not limited to this situation.

Crucial elements of any statistical modelling exercise are model elicitation and specification. For many time series models, and for GNAR in particular, this involves choosing quantities such as the order p, q of any autoregressive and moving average terms, respectively, and the differencing parameter, d. GNAR models also involve p, and, in addition, the $p \times 1$ vector, s: the number of 'stage-neighbours' per lag. Until now, the main tools for GNAR model order choice have been Akaike's and the Bayesian information criteria (AIC and BIC), GNAR versions of which appear in the `GNAR` CRAN package developed by Knight et al. (2023) for `R`, for example.

In regular univariate time series modelling, users benefit from both AIC and BIC, but are aware of their shortcomings, especially for short series. For example, several different models that yield similar AIC/BIC values make it difficult to choose between them. In addition, AIC and BIC computation can be time consuming for models with geometric parameter growth. For example, for an order p global-α GNAR model that admits s stages of neighbours per lag this means estimating $p\,s + p$ parameters. Typically, the 'final' model will be parsimonious, but $2^{p\,(s+1)}$ models might need to be investigated with AIC/BIC until that final model is found. For instance, for monthly data, we might want to start with $p = 12$ to enable detection of annual cycles and with, e.g., $s = 4$ this would result in an unwieldy $2^{12\times 5} \approx 10^{18}$ models to be investigated.

With regular univariate time series, analysts additionally have access to the well–known tools of the autocorrelation (acf) and partial autocorrelation (pacf) functions, which aid model order determination and can also detect other behaviours such as trend, seasonality and non-stationarity. Indeed, acf and pacf plots are often inspected before any formal modelling is attempted. We introduce a new network–enabled version of these tools: Section 3 introduces both the network autocorrelation function (NACF) and the partial NACF (PNACF). Section 3 also introduces a new graphical tool, the Corbit plot, to clearly convey information in either the NACF or PNACF for a network time series (Figure 2 below shows a preview). Corbit plots help users to quickly and directly identify model order and other characteristics of network time series, just as the acf and pacf plots do for univariate series. Section 3 also exhibits Corbit plots on simulated data, clearly showing their advantage for model interpretation and selection.

Section 4 proposes a novel interpretation of GNAR processes as generalised graphical models, which constrains the processes' autoregressive structure and proves some interesting connections to graphical models by incorporating higher–order interactions. Section 4 also proposes a new interpretation of how including prior information into our analysis is related to performing variable selection and shrinkage for GNAR models. In particular, we prove a new result explaining the connection between our multi–stage GNAR neighbourhood structure and a hierarchy imposed on the process' inverse cross–spectrum matrix. Section 4 also shows how classical graphical time series models can be seen as a special case of GNAR processes.

Section 5 proposes a new analysis of the problem of modelling, analysis and prediction of the number of patients occupying mechanical ventilation beds (prevalence) during the COVID–19 pandemic in 140 National Health Service (NHS) Trusts in England. Corbit plots conveniently and rapidly give strong guidance as to choice of GNAR process order that suggests a very parsimonious model. We demonstrate the excellent predictive performance for our fitted GNAR models compared to established time series models, but also their close connections to conditional autoregressive spatial models, but only for the GNAR$(1, [1])$ model.

We further introduce an extension of the Corbit plot, namely the R–Corbit plot, which permits analysts to understand (i) the effect of covariates on the network time series correlation structure and (ii) how the correlation structure can change over different time periods. The latter can provide a clear and immediate indication of nonstationarity, where it exists. For the COVID–19 mechanical ventilation beds time series we find that a R–Corbit plot can show how the dynamics of the process change during different waves of the pandemic. The 'R–' in the name R–Corbit plot highlights that such plots are comprised of rings of circles. We also present two new plots that show the local and global relevance of individual NHS Trusts within the network.

GNAR is an alternative method for time series modelling, which is especially useful when the data satisfy certain conditions, which we make explicit in Sections 2 and 4. Thus, GNAR should be thought of as an addition to the existing toolbox for multivariate time series or spatio–temporal data.

Next, Section 2 formulates a hierarchical representation for GNAR processes, which allows us to write the model in compact matrix notation and later efficiently define the GNAR NACF and PNACF and associated Corbit and R–Corbit plots.

2 GNAR Model and Methods

A network time series $\mathcal{X} := (\boldsymbol{X}_t, \mathcal{G})$ is a stochastic process composed of a multivariate time series $\boldsymbol{X}_t \in \mathbb{R}^d$, $t = 1, \ldots, T$, and an underlying network $\mathcal{G} = (\mathcal{K}, \mathcal{E})$, where $\mathcal{K} = \{1, \ldots, d\}$ is a set of nodes, $\mathcal{E} \subseteq \mathcal{K} \times \mathcal{K}$ is a set of edges, and $\mathcal{G}$ is an undirected graph, which has d nodes (vertices). Each univariate time series $X_{i,t} \in \mathbb{R}$ is associated to node $i \in \mathcal{K}$ in $\mathcal{G}$.

We review the global–α GNAR model for analysing network time series given our particular focus on similar interactions across nodes in the network. We assume that the network is static throughout, although, GNAR processes can handle time–varying networks; see Knight et al. (2016, 2020). We next introduce two matrices that enable to express the GNAR model more compactly.

2.1 Weights and r–stage adjacency matrices

GNAR processes are parsimonious models as they exploit network structure. A key notion is that of r-stage neighbours. We say that nodes i and j are r-stage neighbours if and only if the shortest path on the network $\mathcal{G}$ between them has 'distance' equal to r, in the sense that the number of edges on the shortest path is equal to r, and define $\mathcal{N}_r(i) \subseteq \mathcal{K}$ as the set of r-stage neighbours of node i. We denote this higher–order structure by introducing the r-stage adjacency matrix $\mathbf{S}_r$.

Definition 1. *Let $\delta(i, j)$ be the number of edges between i and j on the shortest path between them, and $(\boldsymbol{X}_t, \mathcal{G})$ be a network time series as above. Define the r–stage adjacency matrix $\mathbf{S}_r \in \mathbb{R}^{d \times d}$ to have entries $[\mathbf{S}_r]_{ij}$, where each entry $[\mathbf{S}_r]_{ij} = 1$ if and only if node i is an r–stage neighbour of node j, otherwise $[\mathbf{S}_r]_{ij} = 0$. That is, $j \in \mathcal{N}_r(i) \iff \delta(i, j) = r \iff [\mathbf{S}_r]_{ij} = 1$.*

The matrix $\mathbf{S}_1$ is the regular adjacency matrix and nodes cannot be r-stage neighbours for different choices of r. Figure 1 illustrates $\mathbf{S}_r$ by plotting the set of r-stage neighbours for $r = 1, 6$ present in the network $\mathcal{G}$ associated to the COVID–19 (network) time series. There are no neighbours at seven stages or higher for this network time series. The set of r-stage neighbours of node i can be found by looking at the ith row of $\mathbf{S}_r$, furthermore, each $\mathbf{S}_r$ is a symmetric matrix that can be computed sequentially from previous r-stage adjacency matrices; see the separate supplementary material document section C for a more thorough exposition.

We also consider weights between nodes i and j: each weight $w_{ij} \in [0, 1]$ quantifies the relevance node j has on node i with respect to neighbourhood regression. If the network $\mathcal{G}$ does not have weighted edges, a GNAR model assigns equal importance to each node j in the set of r-stage neighbours in the sense that if node j is an r-stage neighbour of node i, then $w_{ij} = \{|\mathcal{N}_r(i)|\}^{-1}$.

If $\mathcal{G}$ has weighted edges $\tilde{w}_{ij}$, then each weight is normalised, so that the weights associated to each r-stage neighbourhood sum to one, as follows $w_{ij} = \tilde{w}_{ij}\{\sum_{l \in \mathcal{N}_r(i)} \tilde{w}_{il}\}^{-1}$. Hence, $\sum_{j \in \mathcal{N}_r(i)} w_{ij} = 1$ for all r-stage neighbourhood sets. The connection between these weights and inverse distances is explored in Section 4.2.

A GNAR model performs autoregression for each nodal time series as well as neighbourhood regression. By neighbourhood regression we mean that for each nodal time series $X_{i,t}$

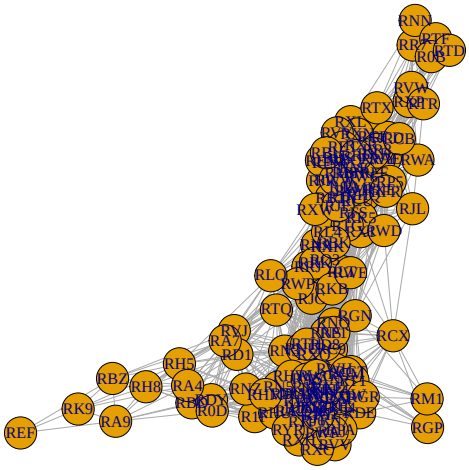

(a) NHS Trusts network 1-stage neighbours.

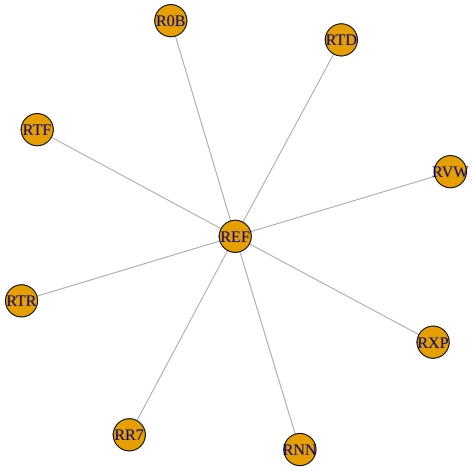

(b) NHS Trusts network 6-stage neighbours.

Figure 1: (a) network with directly connected nodes. (b) network corresponding to 6-stage neighbours. NHS Foundation Trust Codes: REF=Royal Cornwall Hospitals; RVW=North Tees & Hartlepool; RXP=County Durham & Darlington; RNN=North Cumbria Integrated Care; RR7=Gateshead Health; RTR=South Tees Hospitals; RTF=Northumbria Healthcare; R0B=South Tyneside & Sunderland; RTD=Newcastle upon Tyne Hospitals.

we compute its autoregression at lag k with a convex linear combination $Z^r_{i,t}$ of its r-stage neighbours, which for a fixed $r \in \{1, \ldots, r_{\max}\}$ is given by

$$Z^r_{i,t} := \sum_{j \in \mathcal{N}_r(i)} w_{ij} X_{j,t}, \tag{1}$$

where $r_{\max} \in \mathbb{N}$ is the longest shortest path in the network $\mathcal{G}$, i.e. $\delta(i,j) \leq r_{\max}$ for all node pairs (i,j), $i = 1, \ldots, d$ and $t = 1, \ldots, T$. Since node j can only be part of one neighbourhood regression with respect to all other nodes in $\mathcal{G}$ we can identify the unique connection weight between nodes i and j as w_{ij} for all nodes in $\mathcal{G}$. To help express neighbourhood regression in matrix notation we introduce the weights matrix $\mathbf{W}$ for GNAR models.

Definition 2. *Let $\mathcal{G} = (\mathcal{K}, \mathcal{E})$ be a network, then the weights matrix is the matrix $\mathbf{W} \in \mathbb{R}^{d \times d}$ with entries $[\mathbf{W}]_{ij} := w_{ij}$ for $i, j \in \mathcal{K}$.*

Note that the diagonal entries are equal to zero because there are no self–loops in $\mathcal{G}$, and that $\mathbf{W}$ is not necessarily symmetric because nodes can have different degrees of relevance across the network.

2.2 GNAR Model

GNAR models were introduced by Knight et al. (2016). We review them here and additionally introduce the use of a Hadamard operator, which makes the specification more compact and, importantly, permits us to write GNAR as a vector process.

Let $\odot$ denote the Hadamard (component–wise) product, which paired with $\mathbf{S}_r$ and $\mathbf{W}$ can be used to select the set of r-stage neighbours for each node i and compute the corresponding neighbourhood regression $Z^r_{i,t}$. The *node–wise* representation of a global-α GNAR model with maximum lag equal to $p \in \mathbb{N}$ and maximum r-stage depth $s_k \in \{1, \ldots, r_{\max}\}$ at each lag is

$$X_{i,t} = \sum_{k=1}^{p} \left(\alpha_k X_{i,t-k} + \sum_{r=1}^{s_k} \beta_{kr} Z^r_{i,t-k} \right) + u_{i,t}, \tag{2}$$

where $i = 1, \ldots, d$, $t = 1, \ldots, T$, the $\alpha_k \in \mathbb{R}$ are 'standard' autoregressive parameters and the $\beta_{kr} \in \mathbb{R}$ are neighbourhood autoregressive parameters for $r = 1, \ldots, s_k$ at each lag $k = 1, \ldots, p$. The model is denoted GNAR$(p, [s_1, \ldots, s_p])$, which has p autoregressive terms and for each one of these there are s_k neighbourhood regression terms given by (1). The following notational convenience is used when consecutive s_k are identical in the $[s_1, \ldots, s_p]$ vector. For example, we write $[3^{(2)}7^{(5)}]$ for $[3, 3, 7, 7, 7, 7, 7]$ or $[3^{(4)}]$ for $[3, 3, 3, 3]$, *etc.* The latter concise specification is useful when describing an initial full model before, e.g., embarking on backward variable deletion.

Also, we assume that the $u_{i,t}$ is independent and identically distributed (IID) white noise with mean zero and variance $\sigma^2 > 0$ for all nodes. The model given by (2) is a more compact representation of the model in Knight et al. (2016).

Before expressing the model in (2) by a vector-wise representation we introduce the r-stage linear regression vector time series

$$\boldsymbol{Z}^r_t := (\mathbf{W} \odot \mathbf{S}_r) \boldsymbol{X}_t. \tag{3}$$

Each ith entry in $\boldsymbol{Z}_t^r$ is equal to the r-stage neighbourhood regression for node i given by (1). Now we can write the vector notation version of the model in (2) as

$$\boldsymbol{X}_t = \sum_{k=1}^{p} \left(\alpha_k \boldsymbol{X}_{t-k} + \sum_{r=1}^{s_k} \beta_{kr} \boldsymbol{Z}_{t-k}^r\right) + \boldsymbol{u}_t, \tag{4}$$

where $t = 1, \ldots, T$, the $\alpha_k \in \mathbb{R}$ and $\beta_{kr} \in \mathbb{R}$ are the autoregressive coefficients in (2) and $\boldsymbol{u}_t$ are (IID) multivariate white noise with mean zero and covariance matrix $\sigma^2 \mathbf{I_d}$. The representation (4) highlights the parsimonious structure of a global-α GNAR model. Note that the number of parameters in the model increases not with the dimension of $\boldsymbol{X}_t$ and lag, but rather with the depth of r-stage regression and maximum lag.

A close look at (4) reveals that the global-α GNAR model can be written as a constrained Vector Autoregressive (VAR) model; see Brockwell and Davis (2006), for which the autoregressive matrices

$$\boldsymbol{\Phi}_k := \{\alpha_k \mathbf{I_d} + \sum_{r=1}^{s_k} \beta_{kr} (\mathbf{W} \odot \mathbf{S}_r)\},$$

are restricted by the network structure. Knight et al. (2020) exploit this connection to show a more general result with respect to stationarity conditions for GNAR processes with a static network than the one we give below.

Theorem 1. *[**Knight et al. (2020)**] Let $\boldsymbol{X}_t$ be a global-α GNAR$(p, [s_1, \ldots, s_p])$ process with associated static network $\mathcal{G} = (\mathcal{K}, \mathcal{E})$. If the autoregressive coefficients in (4) satisfy*

$$\sum_{k=1}^{p} (|\alpha_k| + \sum_{r=1}^{s_k} |\beta_{kr}|) < 1,$$

then $\boldsymbol{X}_t$ is stationary.

We end by highlighting that GNAR models can be viewed as highly parsimonious VAR models with parameter constraints informed by the underlying network structure. If a GNAR formulation is appropriate for modelling a particular data set, then it can be an extremely powerful forecasting tool, as previously noted (Knight et al., 2020; Nason and Wei, 2022), which enables interpretation of a large number of interactions. We describe these properties in Section 4 and illustrate its advantages by analysing the COVID–19 (network) time series in Section 5.

2.3 GNAR Model Estimation

The original GNAR work (Knight et al., 2016) estimated parameters using least squares. Expression as a formal linear model was established by Leeming (2019) and soon implemented by Knight et al. (2023). To introduce notation and to enable us to properly describe our new connection between GNAR modelling and variable shrinkage and selection in Section 4, we present a slightly modified and expanded description here.

A global–α GNAR$(p, [s_1, \ldots, s_p])$ model has p autoregressive α_k coefficients and $\sum_{k=1}^{p} s_k$ neighbourhood regression β_{kr} coefficients. For comparison, a VAR(p) model has pd^2 parameters, so as long as $q := p + \sum_{k=1}^{p} s_k < pd^2$ the GNAR model (4) needs to estimate far

fewer parameters. This is particularly important for settings in which pd^2 is larger than the number of time step realisations observed, such as the COVID–19 data we analyse below.

Assume that $T \in \mathbb{N}$ time steps of data $\mathbf{X} := [\boldsymbol{X}_1, \ldots, \boldsymbol{X}_T]$ arising from a GNAR process with known order become available. Our objective is to estimate the unknown autoregressive coefficients α_k and β_{kr} after fixing the lag–depth pair $(p, [s_1, \ldots, s_k])$.

To do this we assume that $\boldsymbol{X}_t$ is a stationary GNAR$(p, [s_1, \ldots, s_p])$ process, and that $n = T - p$ is the number of observations for which there are p previous observed lags available for estimation, and, for $t = p+1, \ldots, T$, define the following.

$$\begin{aligned} \boldsymbol{y}_t &:= \boldsymbol{X}_{p+1}, \\ \mathbf{Z}_{t-1}^{1:s_1} &:= [\boldsymbol{Z}_{t-1}^1, \ldots, \boldsymbol{Z}_{t-1}^{s_1}], \\ \mathbf{R}_t &:= [\boldsymbol{X}_{t-1}, \mathbf{Z}_{t-1}^{1:s_1}, \ldots, \boldsymbol{X}_{t-p}, \mathbf{Z}_{t-p}^{1:s_p}], \end{aligned} \tag{5}$$

where $\boldsymbol{y}_t \in \mathbb{R}^d$ is the data vector of 'responses', $\mathbf{R}_t \in \mathbb{R}^{d \times q}$ is the design matrix at time-step t, and $\boldsymbol{Z}_{t-1}^{s_1}$ are given by (3). Furthermore, define the vector of parameters $\boldsymbol{\theta} \in \mathbb{R}^q$ as

$$\boldsymbol{\theta} := (\alpha_1, \beta_{11}, \ldots, \beta_{1s_1}, \alpha_2, \ldots, \beta_{ps_p}),$$

which are the unknown linear model coefficients.

Thus, if $\boldsymbol{\theta}$ satisfies the assumptions in Theorem 1, the realisations $\boldsymbol{y}_t = \mathbf{R}_t\,\boldsymbol{\theta} + \boldsymbol{u}_t$ are statistically uncorrelated observations of linear models given by (4), where $\boldsymbol{u}_t$ are the same as in (4) for $t = p+1, \ldots, T$. Next, by concatenating both the column vectors $\boldsymbol{y}_t$ into one column vector $\boldsymbol{y} \in \mathbb{R}^{nd}$ and the design matrices $\mathbf{R}_t$ into one design matrix $\mathbf{R} \in \mathbb{R}^{nd \times q}$, we can write (4) as the linear model

$$\boldsymbol{y} = \mathbf{R}\,\boldsymbol{\theta} + \boldsymbol{u}. \tag{6}$$

Now, we can couple the n linear regression problems as if we had n independent samples of size d and fit the linear model by ordinary least squares for data with sample size equal to nd and q unknown parameters, thus, the least squares estimator for a GNAR$(p, [s_1, \ldots, s_p])$ model with a global-α specification is given by

$$\hat{\boldsymbol{\theta}} = \left(\mathbf{R}^T\,\mathbf{R}\right)^{-1}\mathbf{R}^T\boldsymbol{y}, \tag{7}$$

where $\mathbf{R}$ and $\boldsymbol{y}$ are given by (5).

If we further assume that the $\boldsymbol{u}_t \sim N(0, \sigma^2\mathbf{I_d})$, then $\hat{\boldsymbol{\theta}}$ given by (7) is also the conditional maximum likelihood estimator. We also point out that assuming that all the nodal white noise processes have the same variance might not be sensible, in that case it is possible to adapt (6) into a generalised least squares problem, and other relaxations are possible. Nevertheless, throughout this work we maintain the assumptions in Theorem 1 and (4), and estimate the unknown coefficients with $\hat{\boldsymbol{\theta}}$ given by (7).

3 New Graphical Aids for Model Selection

This section introduces a network analogue of the autocorrelation and partial autocorrelation function from classical time series. Our network autocorrelation function (NACF) reveals the autocorrelation structure for different choices of maximum h-lag and r-stage depth, which we denote by (h, r). We introduce the correlation-orbit (Corbit) plot that

displays NACF values and also serves as an effective graphical aid to perform model selection, namely selecting good values of (h, r). The NACF depends not only on the stochastic values of the multivariate time series in a network time series, but also takes account of the network structure and weights.

3.1 GNAR Network Autocorrelation Function

Recall the familiar autocorrelation, $\rho(h)$, for a univariate time series $X_t \in \mathbb{R}$ for lags h:

$$\rho(h) = \frac{\sum_{t=1}^{T-h}(X_{t+h} - \overline{X})(X_t - \overline{X})}{\sum_{t=1}^{T}(X_t - \overline{X})^2}. \tag{8}$$

This autocorrelation, $\rho\,(h)$, computes the covariance between (a mean-corrected) X_t and its h–lagged value, X_{t+h} and then normalises by the sample variance in the denominator of (8). The usual T^{-1} covariance and variance scale normalisations in the numerator and denominator of (8) cancel, see Chatfield (2004, Section 2.7)

Our network autocorrelation, nacf, has a similar basic structure to ρ with two main differences. The first difference is that we examine network autocorrelations not only at time lag h but also for a given r-stage neighbour, so nacf = nacf(h, r). The second difference occurs because the GNAR model (3) involves not just past values of $\boldsymbol{X}_t$ but *weighted* past values of neighbours and hence those weights need to be incorporated as the following definition shows.

Definition 3 (Network Autocorrelation Function (NACF))**.** *Suppose that $\boldsymbol{X}_t$ is a GNAR process as defined by* (3) *that satisfies the conditions in Theorem 1. Further, let $\mathbf{S}_r$ and $\mathbf{W}$ be the r-stage adjacency and weight matrices as defined in Definitions 1 and 2, respectively. The network autocorrelation function of a* GNAR *process $\boldsymbol{X}_t$, with autocovariance bound $\lambda := \left[\max_{j=1,\ldots,d}\left\{\sum_{i=1}^{d}[(\mathbf{W}\odot\mathbf{W})]_{ij}\right\}\right]^{1/2}$, is given by*

$$\mathrm{nacf}(h, r) := \frac{\sum_{t=1}^{T-h}(\boldsymbol{X}_{t+h} - \overline{\boldsymbol{X}})^T\big(\mathbf{W}\odot\mathbf{S}_r + \mathbf{I_d}\big)(\boldsymbol{X}_t - \overline{\boldsymbol{X}})}{\sum_{t=1}^{T}(\boldsymbol{X}_t - \overline{\boldsymbol{X}})^T\big\{\big(1+\lambda\big)\mathbf{I_d}\big\}(\boldsymbol{X}_t - \overline{\boldsymbol{X}})}, \tag{9}$$

where $\mathbf{I_d}$ is the d-dimensional identity matrix.

The rth stage neighbour selection and weighting of those in the nacf is achieved by the term $\mathbf{W}\odot\mathbf{S}_r$ in the numerator of (9). The direct comparison of $\boldsymbol{X}_{t+h}$ to its predecessors, analogous to the numerator in (8) is enabled by the $\mathbf{I_d}$ term in the numerator of (9). The introduction of the $\mathbf{W}\odot\mathbf{S}_r$ term in the numerator of (9) can be thought of as a potential 'inflation' over the standard numerator and so, to ensure that $-1 \leq \mathrm{nacf}(h, r) \leq 1$ we need to modify the denominator. We achieve this by computing the all-encompassing autocovariance bound λ, which includes all weights and hence bounds any $\mathbf{S}_r$-selected neighbour weights that might appear in the numerator. Incidentially, the nacf for a trivial GNAR model with a single node network reduces to the ordinary autocorrelation, i.e. nacf(h, r) = $\rho\,$(h).

For model selection we can employ NACF on a similar basis to that for the regular autocorrelation for univariate time series. By comparing the NACF values for different

choices of (h, r) we can analyse the lag and r-stage depth at which autocorrelation starts to decay. We explore a possible NACF interpretation in Section 4.3; see the supplementary material document Section A for the NACF derivation and some of its properties.

3.2 Corbit Plot

We introduce the Corbit plot by studying realisations coming from a stationary global-α GNAR$(2, [1, 1])$ process with parameters $\alpha_1 = 0.23, \alpha_2 = 0.11, \beta_{1,1} = 0.21$ and $\beta_{2,1} = 0.12$. Assume that we do not know the model order: we can study the network autocorrelation decay by plotting the observed NACF values via the Corbit plot.

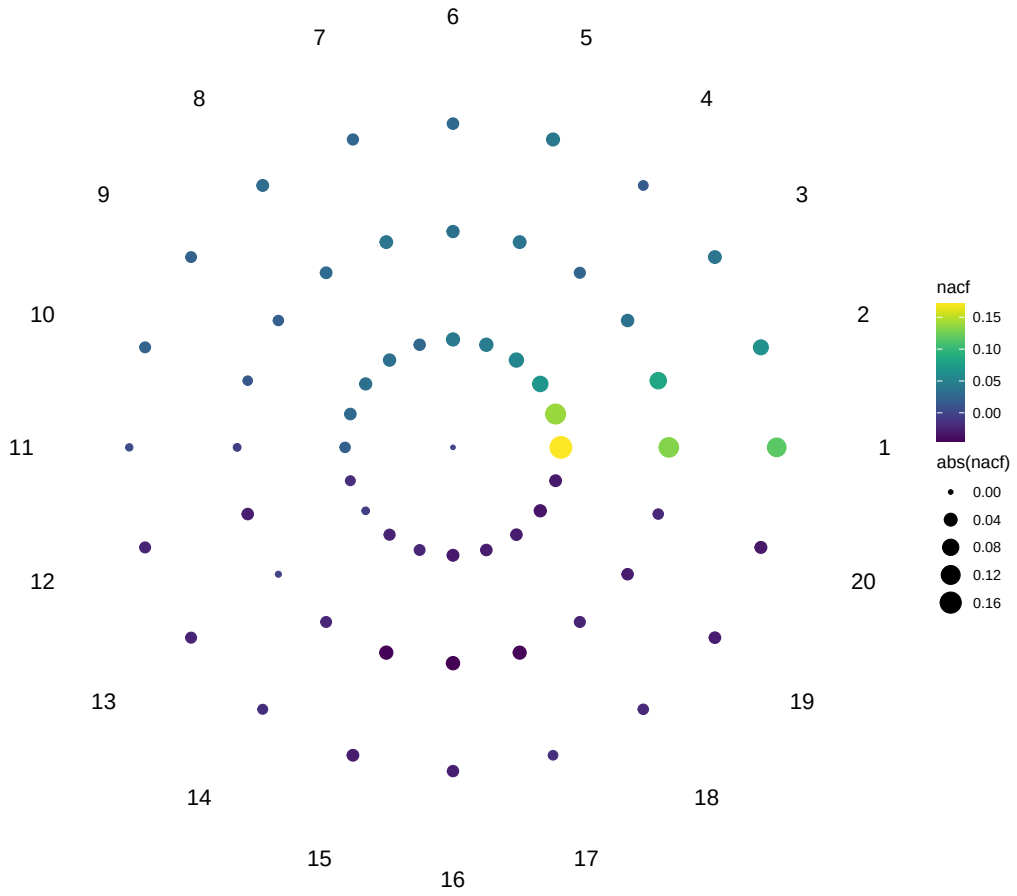

Figure 2: Corbit NACF plot for $T = 200$ samples from a stationary global–α GNAR$(2, [1, 1])$, where the underlying network is the fiveNet network included in the `GNAR` package; see Knight et al. (2023). See text for description.

Figure 2 introduces the Corbit plot, each point corresponds to a specific h-lag and r–stage pair, and the colour is set by a colour scale based on the overall NACF values. The first ring depicts 1–stage neighbours (i.e., nodes with one edge between them), the second ring considers 2–stage neighbours (i.e., nodes with a shortest path length equal to two). In short, the ring number counting from the inside corresponds to r-stage depth.

The numbers on the outside ring indicate the time lag used for computing the NACF. Therefore, the value of each point is $\text{nacf}(h, r)$ where h is the lag denoted on the the last ring and r is the ring that corresponds to r–stage adjacency.

The point on the first inner ring with a number one to the right in Figure 2 is the value of $\text{nacf}(1, 1)$, the second point on the first inner ring is $\text{nacf}(2, 1)$, and the first point on the second inner ring is $\text{nacf}(1, 2)$; this pattern repeats for subsequent rings and lags.

Currently, in our software, there are two possible ways for assigning size to each point. The default choice is to use the NACF absolute value, i.e., $|\text{nacf}(h, r)|$. This choice highlights the different $\text{nacf}(h, r)$ magnitudes. An alternative choice is based on the residual sum of squares constraining GNAR to a specific lag and stage pair produces; see the supplementary material. The value of the largest correlation in Figure 2 is about 0.14, which might seem a bit small. This is because the correlations are weighted by the (usually inverse distance) weights matrix $\mathbf{W}$, which sum to one for a given node. So, the pairs that make up the correlation are weighted by numbers between zero and one, and hence overall they are generally smaller. The autocovariance bound in Definition 3 also reduces the correlations a little. Examples with larger correlations can be found in the associated RMarkdown document Section 2.

Finally, the point at the centre has NACF value equal to zero and the smallest size, which highlights the larger NACF values and facilitates comparing the NACF values to $\text{nacf}(h, r) = 0$. We note that these choices are not exclusive and other measures of model fit and/or correlation could be used for assigning point size and colour.

Corbit plots are produced using the `viridis` R library, which provides a colour scale that is easily perceived by viewers with common forms of colour blindness (Garnier et al. (2023)) and the `ggplot` package functionality (Wickham (2016)). The `corbit_plot` function in the `GNAR` package can also produce other versions of the plot — one with a line between the highest lag and lag 1 to indicate that these lags are not in actuality close, and also a rectangular version, see Figures 9 and 10 in Appendix B below.

The Corbit plot in Figure 2 shows that the NACF decays on/after lags equal to or larger than four across all stages. Also, the NACF drops after the second stage at the first lag and after the first stage for the second lag. Observe that the further separated nodes are in the network the closer the NACF is to zero. Furthermore, across all r-stage depths we see that the NACF decays to zero as the lag increases. This Corbit plot suggests that autocorrelation for the simulated network time series has larger values for $h \in \{1, 2\}$ and $r \in \{1, 2, 3\}$ and decays sharply as the h-lag and r-stage depth increase.

This is in accordance with univariate ACF plots which decay as the lag increases, and does reflect the known underlying GNAR$(2, [1, 1])$ structure.

3.3 GNAR Partial Autocorrelation Function

The NACF computes the autocorrelation between $\boldsymbol{X}_t$ and its lagged observations for a specific choice of r-stage neighbourhood regression, however, it does not account for the effects previous and intervening lags and/or r-stage neighbours have when computing $\text{nacf}(h, r)$. This makes diagnosing model order by looking at the NACF values on a Corbit plot challenging since we do not know if autocorrelation has not reduced because of the effects previous lags and/or r-stage depths might have. This difficulty could prevent us from observing the underlying GNAR autocorrelation structure if there is one.

Motivated by techniques from univariate time series analysis, we propose the partial network autocorrelation function (PNACF) as a tool for diagnosing GNAR model selection. The PNACF computes the autocorrelation between $\boldsymbol{X}_t$ and h-lagged observations of itself for a specific r-stage neighbourhood regression after the linear effects of previous lags and r-stage neighbours have been removed. The PNACF acts as the partial autocorrelation function does for univariate time series by identifying model order from examining the (h, r) pair after which there is a sharp decline in autocorrelation.

Assume that $\boldsymbol{X}_t$ is a GNAR model given by (4) and satisfies the conditions in Theorem 1, then it is possible to remove the effects from previous lags and r-stage neighbours by focusing on the empirical residuals arising from a GNAR$(h-1, [(r-1)^{(h-1)}])$ fit. These residuals correspond to the best linear prediction restricted to lag $(h-1)$ and maximum r-stage depth $(r-1)$, which we denote by $\boldsymbol{X}_t^{h-1,r-1} := \sum_{k=1}^{h-1}(\hat{\alpha}_k \boldsymbol{X}_{t-k} + \sum_{s=1}^{r-1} \hat{\beta}_{kr} \boldsymbol{Z}_{t-k}^{r-1})$; see the Definition 2 in the separate supplementary material document.

One possible extension of the PACF from a univariate setting to the GNAR framework is defining the PNACF as the NACF between the residuals arising from the best linear predictions using $(h-1)$ lags and $(r-1)$ r-stage neighbourhood regressions for h-lag and r-stage pairs. Unfortunately, computing the PNACF as mentioned above requires us to have prior knowledge of the autoregressive coefficients in (4). We circumvent this by inputting the least-squares estimators as if they were the true parameter values, which is valid given the consistency of the estimator given by (7); see Knight et al. (2020). The values we get using the imputed parameters should reflect the underlying GNAR autocorrelation structure if there is one. The new forecast value is $\hat{\boldsymbol{X}}_t^{h-1,r-1} := \sum_{k=1}^{h-1}(\hat{\alpha}_k \boldsymbol{X}_{t-k} + \sum_{s=1}^{r-1} \hat{\beta}_{ks} \boldsymbol{Z}_{t-k}^{s})$. Our PNACF is defined below.

Definition 4. *For a stationary* GNAR *process* $\boldsymbol{X}_t$ *compute the residuals coming from a* GNAR$(h-1, [(r-1)^{(h-1)}])$ *fit, the corresponding residual mean* $\overline{\boldsymbol{u}}$*, and the residuals with* h*-lags between them by* $\hat{\boldsymbol{u}}_{t+h} = \boldsymbol{X}_{t+h} - \hat{\boldsymbol{X}}_{t+h}^{h-1,r-1}$ *and* $\hat{\boldsymbol{u}}_t = \boldsymbol{X}_t - \hat{\boldsymbol{X}}_t^{h-1,r-1}$*. Then, the sample partial network autocorrelation function is*

$$\text{pnacf}(h, r) := \frac{\sum_{t=1}^{T-h}(\hat{\boldsymbol{u}}_{t+h} - \overline{\boldsymbol{u}})^T \big(\mathbf{W} \odot \mathbf{S}_r + \mathbf{I_d}\big)(\hat{\boldsymbol{u}}_t - \overline{\boldsymbol{u}})}{\sum_{t=1}^{T}(\hat{\boldsymbol{u}}_t - \overline{\boldsymbol{u}})^T \big\{\big(1+\lambda\big)\mathbf{I_d}\big\}(\hat{\boldsymbol{u}}_t - \overline{\boldsymbol{u}})}, \tag{10}$$

where λ *is the same as in Definition 3.*

The PNACF computes the remaining network autocorrelation between residuals after removing the linear effects of previous lags and stages. Intuitively, it will cut–off to zero at every (h, r) pair where $h > p$ and $r > r^*$, where $r^* := \max\{s_1, \ldots, s_p\}$ is the largest active r-stage depth, since these pairs correspond to the sum of cross-correlations between the IID white noise processes $u_{i,t+h}$ and $u_{j,t}$ given by (2). By computing said network autocorrelations, the PNACF highlights the stage and lag at which the network autocorrelation 'cuts off'.

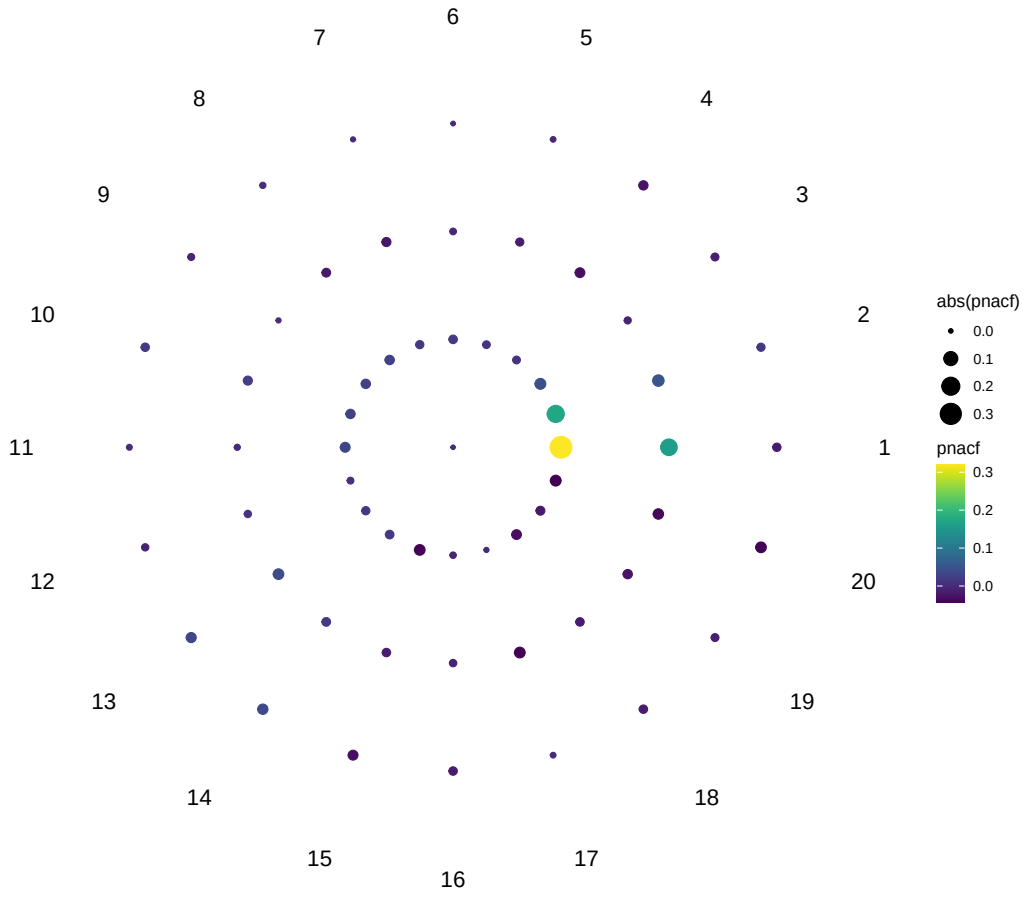

Figure 3: Corbit PNACF plot for $T = 200$ samples from a stationary global-α GNAR$(2, [2, 1])$ which has the fiveNet network as underlying structure; see Knight et al. (2023). The maximum lag is equal to 20 and maximum r-stage is equal to 3.

Figure 3 shows that the PNACF cuts–off at lag three across all stages and indeed it cuts off for all r-stage depths for $h \geq 3$), and that it 'cuts off' at stage one for lag two and at stage two for lag one. This Corbit plot suggests fitting a GNAR$(2, [2, 1])$ which recovers the known data–generating process in this case. Note that the PNACF cut–off mimics the way in which the PACF decays when looking at univariate time series; see Brockwell and Davis (2006). We will introduce the R–Corbit plot below, which is a development of the Corbit plot that highlights non–stationarities or indicates the effect of covariates.

4 GNAR Properties and Useful New Interpretations

GNAR processes generalise graphical models for multivariate time series by introducing higher–order interactions between nodes, and resulting in a parsimonious specification that leverages the similarities of the individual node–wise processes. For our COVID–19 pandemic analysis later, it is reasonable to expect that the SARS–CoV–2 virus behaves similarly in different locations across England. This section introduces novel explicit connec-

tions between GNAR and graphical models for multivariate time series and further explains new selection and shrinkage properties that GNAR models implicitly possess due to their incorporation of prior knowledge.

4.1 Connection to Graphical Models for Time Series

A goal of GNAR modelling is to include possible interactions between nodes that are not directly connected in the network. One possible way of generalising the notions in Dahlhaus (2000) is to extend edge–based interactions by assigning r-stage adjacency based on a cross–spectral hierarchy presented in this subsection. GNAR introduces higher-order interactions into the graphical model by allowing r-stage neighbourhood regression for $r \in \{1, \dots, r^*\}$, where r^* is the largest active r-stage neighbourhood regression.

These higher–order interactions can be interpreted as weaker dependence between nodes the further separated the nodes are in the graph, in the sense that r-stage neighbourhood regression is less relevant the larger r is and ultimately non-relevant if $r > r^*$. Here, the idea of an edge between nodes is extended to membership in r-stage adjacency sets. Denote by $\mathcal{N}_r$ the set of r-stage neighbours, so if $j \in \mathcal{N}_r(i)$, then, by symmetry and shortest path uniqueness, $(i, j) \in \mathcal{N}_r$, moreover, note that $\mathcal{N}_1$ is the ordinary set of edges.

An intuition for GNAR is that the cross–correlation between $X_{i,t+h}$ and $X_{j,t}$ at all lags h should be strongest if $j \in \mathcal{N}_1(i)$, drop for $j \in \mathcal{N}_r(i)$ where $r \in \{2, \dots, r^*\}$, and that $X_{i,t+h}$ and $X_{j,t}$ do not heavily influence each other if $j \notin \mathcal{N}(i)$, where $\mathcal{N}(i) := \cup_{r=1}^{r^*} \mathcal{N}_r(i)$ is the r^*-borough of node i (i.e., collection of neighbourhoods). This motivation relates r-stage neighbourhood regression to the cross–spectrum and the inverse spectral matrix, as the new result shows next.

Theorem 2. *Let $\boldsymbol{X}_t$ be a stationary* GNAR$(p, [s_1, \dots, s_p])$ *process with a static network structure $\mathcal{G} = (\mathcal{K}, \mathcal{E})$, full rank spectral matrix $\mathbf{f}(\omega)$ and maximum active r-stage depth r^*. Then, the inverse spectral matrix $\mathbf{S}(\omega)$ and the node-wise distances $\delta(i, j)$ computed on the network $\mathcal{G}$ satisfy*

a. There exists a partial correlation graph $\tilde{\mathcal{G}} = (\mathcal{K}, \tilde{\mathcal{E}})$ with the same set of nodes as $\mathcal{G}$ such that

$$(i, j) \notin \tilde{\mathcal{E}} \text{ if and only if } \delta(i, j) \geq 2r^* + 1.$$

b. There exists a cross-spectral hierarchy $\xi^{(1)} > \cdots > \xi^{(r^*)} > \xi^{(r^*+1)} = 0$ and an active r-stage neighbourhood regression which satisfy

$$\delta(i, j) \in \{2r - 1, 2r\} \text{ if and only if } \xi^{(r)} \leq |[\mathbf{S}(\omega)]_{ij}| < \xi^{(r-1)},$$

for all $\omega \in (-\pi, \pi]$ and for all $r \in \{1, \dots, r^*\}$.

See the supplementary material document (Section D) for a proof of Theorem 2, and Brockwell and Davis (2006); Shumway (2017) for definitions of $\mathbf{S}(\omega)$ and $\mathbf{f}(\omega)$. Theorem 2 shows that $X_{i,t}$ and $X_{j,t+h}$ are uncorrelated at all lags h given all the other nodes if and only if nodes i and j do not have common active r-stage neighbours. It extends the notion that nodes without edges between them in a graph are uncorrelated given all the other nodes in said graph, by proposing that if the distance between nodes i and j is larger than $2r^* + 1$, then $X_{i,t}$ and $X_{j,t+h}$ are uncorrelated given all the other nodal time series at all lags, which we express as nodes i and j do not collide in r-stage neighbourhood regression. The ideas in this subsection underpin the node relevance statistics in Section 5.4.

Moreover, Theorem 2 exhibits that the higher-order autocorrelation structure a GNAR process induces is equivalent to the process having a hierarchical dependence structure, which can be identified from the inverse spectral matrix (i.e., $\mathbf{S}(\omega)$ acts similarly as the concentration matrix does for Gaussian graphical models). This property allows us to interpret the relevance different nodes j have with respect to node i by looking for the r-stage neighbourhood regressions at which j is active (i.e., if $j \in \mathcal{N}_r(i)$, then the smaller r is the more relevant j is). Note that if we restrict GNAR to 1-stage neighbourhood regression, then higher-order interactions are not considered and the GNAR induced correlation structure is equivalent to a graphical model for multivariate time series. In that case, Theorem 2 recovers results of Dahlhaus (2000) for partial correlation graphs.

4.2 Oracle Selection and Shrinkage

Prior knowledge of the network can be interpreted as having an oracle solution for selecting active nodes in each r-stage neighbourhood regression. A GNAR formulation exploits this by proposing a reparameterization of a constrained VAR process in a parsimonious manner that is related to autoregressive coefficient shrinkage, which reduces estimator variance and improves model interpretability. We explain this novel interpretation next.

For Selection

Before performing selection, each node–wise autoregression includes all possible nodes as predictors and the equivalent non-constrained VAR(p) model is

$$X_{i,t} = \sum_{k=1}^{p} \left(\phi_k^{ii} X_{i,t-k} + \sum_{j \neq i} \phi_k^{ij} X_{j,t-k} \right) + u_{i,t}, \tag{11}$$

where ϕ_k^{ij}, $\phi_k^{ii} \in \mathbb{R}$ are autoregressive coefficients and the $u_{i,t}$ are IID white noise.

Model (11) has d non-zero coefficients for each node-wise autoregression at every lag, hence, the total number of unknown parameters is $p\,d^2$. Following Hastie et al. (2017), we say that a node-wise regression is m-sparse if only a subset of m predictor nodes have a non-zero autoregressive coefficient. By definition we have that $m \leq d$, however, our focus is on models which highlight a small subset of relevant node predictors (i.e., $m \ll d$). Next, we constrain the VAR model (11) by assuming that only nodes which satisfy $\delta(i,j) \leq r^*$, where the distances are computed on the underlying network, have a non-zero coefficient. Essentially, for all lags $k \in \{1, \ldots, p\}$ we impose the constraint

$$\phi_k^{ij} \neq 0 \text{ } \textit{if and only if} \text{ } \delta(i,j) \leq r^*, \tag{12}$$

by symmetry, we also have that $\phi_k^{ij} \neq 0$ if and only if $\phi_k^{ji} \neq 0$ at all lags k.

Applying constraint (12) to the VAR model (11) and noting that $j \in \mathcal{N}(i)$ if and only if $\delta(i,j) \leq r^*$ gives

$$X_{i,t} = \sum_{k=1}^{p} \left(\phi_k^{ii} X_{i,t-k} + \sum_{j \in \mathcal{N}(i)} \phi_k^{ij} X_{j,t-k} \right) + u_{i,t}, \tag{13}$$

where $\mathcal{N}(i) = \cup_{r=1}^{r^*} \mathcal{N}_r(i)$ and the $u_{i,t}$ are IID white noise. Above, each ith nodal time series has at most $m^{(i)} := |\mathcal{N}(i)| + 1 \leq d$ non-zero autoregressive ϕ_k^{ij}, ϕ_k^{ii} coefficients at each lag

k. Thus, under constraint (12), each node–wise regression is $m^{(i)}$-sparse at each lag and has at most $p\,m^{(i)}$ unknown parameters.

We set $m := \max\{m^{(i)}\}$ and see that all node–wise autoregressions are m–sparse and that the model has at most $p\,m^2$ unknown parameters. Furthermore, constraint (12) performs variable selection for all node-wise autoregressions, and reflects our assumption of closer nodes being more relevant to each other.

Variable selection can be performed by multiplying the vector time series by the sum of r-stage adjacency matrices. Let $\mathbf{S} = \sum_{r=1}^{r^*} \mathbf{S}_r$, and note that $[\mathbf{S}]_{ij} \neq 0$ if and only if $\delta(i,j) \leq r^*$, and that $[\mathbf{S}]_{ii} = 0$ for all nodes i, hence, model (13) is equivalent to

$$X_{i,t} = \sum_{k=1}^{p} \left(\phi_k^{ii} X_{i,t-k} + \sum_{j=1}^{d} \phi_k^{ij} [\mathbf{S}]_{ij} X_{j,t-k} \right) + u_{i,t}, \tag{14}$$

which has the same active nodes (i.e., $\phi_k^{ij}[\mathbf{S}]_{ij} \neq 0 \iff \delta(i,j) \leq r^*$) as the GNAR vector-wise representation (4). This establishes variable selection equivalence between a GNAR formulation and a constrained VAR, where the number of selected nodes for each node-wise autoregression satisfies $m^{(i)} = \sum_{j=1}^{d} [\mathbf{S}]_{ij}$.

Moreover, fixing r^* in a GNAR formulation is equivalent to imposing a ℓ_0-ball constraint on the autoregressive coefficients, which can be efficiently approximated by an ℓ_1-norm constraint; see Chapter 7.2.1 in Wainwright (2019). Further, decreasing r^* reduces the number of nodes included in node-wise autoregressions, which results in a sparser model by noting that at all lags k

$$0 < \|\mathbf{\Phi}_k \odot \mathbf{S}_1\|_1 \leq \nu^{(1)} \leq \cdots \leq \|\mathbf{\Phi}_k \odot \mathbf{S}\|_1 \leq \nu < \|\mathbf{\Phi}_k\|_1 ,$$

hence, as r^* decreases the number of active nodes decreases too, which results in a smaller $\nu > 0$ (i.e., a tighter constraint) and a sparser model.

Based on the above, we interpret r-stage neighbours as the relevant predictors each node has, and we can think of maximum r-stage depth (i.e., r^*) as a hyperparameter that controls variable selection.

For Shrinkage

GNAR accounts for the possibility that nodes in the same $\mathcal{N}_r$ are likely to be correlated, which will affect estimator and predictive performance (under a valid GNAR model); see Chapter 3 in Hastie et al. (2017). Motivated by this, a GNAR formulation performs shrinkage on the selected variables at the population level by reparametrizing the constrained VAR model as follows.

Using the notation and concepts from a GNAR formulation the node–wise autoregressions in a sparse VAR(p) are given by (13). We assume that relevance weights $\sigma_{ij} > 0$ between nodes are available, which quantify the similarity between nodes i and j, and can be computed as $\sigma_{ij} := \{h(i,j)\}^{-1}$, where $h(i,j) > 0$ measures a notion of distance between nodes, which does not have to be equal to the distance in the graph (but could be), for instance, the distance can be a function of some exogenous variable that measures 'closeness' between nodes in a non–linear manner. Essentially, the σ_{ij} are a form of hard prior knowledge.

The notion of closeness and 'similarity' between nodes that the σ_{ij} provide can be incorporated into the GNAR framework by reparameterizing the autoregressive coefficients in (13) as $\beta_{kr}\,\sigma_{ij} := \phi_k^{ij}\,[\mathbf{S}]_{ij}$, where prior knowledge of σ_{ij} makes the β_{kr} identifiable. Also, it means that if $\delta(i,j) > r^*$, then $\beta_{kr}\,\sigma_{ij} = 0$. This parameterization assumes that there is a global effect β_{kr} common across r-stage neighbours, which results in a parsimonious representation, i.e., a GNAR model is valid.

To satisfy the assumptions of Theorem 1 (i.e., weights less than or equal to one), we normalise the weights by computing updates as $w_{ij} := \sigma_{ij}(\sum_{l\in\mathcal{N}_r(i)}\sigma_{il})^{-1}$, hence, $\sum_{j\in\mathcal{N}_r(i)} w_{ij} = 1$ for all nodes at every active r-stage neighbourhood regression. Finally, to transform (13) into a model equivalent to a GNAR model shrink the active ϕ_k^{ij} coefficients as follows

$$\gamma_k^{ij} := \phi_k^{ij}\,\{1 + \sigma_{ij}^{-1}\,v_r(i,j)\}^{-1}, \tag{15}$$

where $v_r(i,j) := \sum_{l\in\mathcal{N}_r(i)-\{j\}}\sigma_{il}$ - i.e., weight normalisation can be thought of as a constraint on the ℓ_2-norm of the active coefficients. We further note an interesting connection between the above and parameter updates in linear ridge regression.

Proposition 1. *Let $\boldsymbol{y} \in \mathbb{R}^n$ be a vector of responses, $\mathbf{A} \in \mathbb{R}^{n\times m}$ the design matrix and $\boldsymbol{\phi} \in \mathbb{R}^m$ the vector of unknown linear coefficients. Next define $\hat{\boldsymbol{\phi}} := \arg\min\{||\boldsymbol{y} - \mathbf{A}\,\boldsymbol{\phi}||_2^2\}$, and $\hat{\boldsymbol{\gamma}} := \arg\min\{||\boldsymbol{y} - \mathbf{A}\,\boldsymbol{\gamma}||_2^2\}$ such that $||\boldsymbol{\gamma}||_2 \leq \lambda$, where $\boldsymbol{\gamma} \in \mathbb{R}^m$ and $\lambda > 0$. If the design matrix admits the singular value decomposition $\mathbf{A} = \mathbf{U}\,\boldsymbol{\Sigma}\,\mathbf{V}^T$, then we have that*

$$\hat{\gamma}_j = \hat{\phi}_j\,(1 + v\,\sigma_j^{-2})^{-1}, \tag{16}$$

where σ_j^2 are the diagonal entries in $\boldsymbol{\Sigma}^2$ and $v > 0$ is the Lagrange multiplier linked to the constraint $||\boldsymbol{\gamma}||_2 \leq \lambda$.

In view of Proposition 1, and by comparing (15) with (16), we interpret each ith node-wise r-stage neighbourhood regression as a sparse linear regression with shrunken coefficients, which satisfy the weight normalisation constraint $\gamma_k^{ij} = \phi_k^{ij}\,\{1 + \sigma_{ij}^{-1}\,v_r(i,j)\}^{-1}\,[\mathbf{S}]_{ij}$ for all nodal pairs at all lags. Moreover, by (15) and the above, the usual estimated GNAR coefficients can thus be re-expressed by a particular transformed and shrunk version of VAR coefficients that we have just explicitly represented by $\gamma_k^{ij} = \beta_{kr}\,w_{ij}$.

As above, the $\beta_{kr}\,w_{ij}$ are the node–wise coefficients in the GNAR parameterization given by (2), which is a constrained reparametrization of the sparse VAR(p) process (13) with shrunken coefficients γ_k^{ij}. This reparametrization results in a parsimonious model with $p + \sum_{k=1}^{p} s_k \ll p\,m^2 \ll p\,d^2$ unknown parameters. Hence, GNAR processes can be interpreted as constrained VAR models which exploit knowledge of the underlying network structure to perform variable selection and shrinkage at the population level. Our GNAR framework produces parsimonious models that are highly interpretable.

4.3 NACF Interpretation

The connection between GNAR processes, graphical models for multivariate time series and sparse VAR models allows us to interpret the NACF as a measure of the constrained (i.e., network–induced) correlation structure in the process. This effect is accounted for by the autocovariance bound λ given by Definition 3.

The sparseness and shrinkage properties GNAR models have permit us to bound the dot product $\langle \boldsymbol{x}, (\mathbf{W} \odot \mathbf{S}_r + \mathbf{I_d})\tilde{\boldsymbol{x}} \rangle$ for all r-stage neighbourhood regressions as follows

$$\left| \left\langle \boldsymbol{x}, (\mathbf{W} \odot \mathbf{S}_r + \mathbf{I_d})\tilde{\boldsymbol{x}} \right\rangle \right| \leq (1 + \lambda) \left\| \boldsymbol{x} \right\| \left\| \tilde{\boldsymbol{x}} \right\|, \tag{17}$$

which illustrates the inner workings of the NACF; see the supplementary material document (Proposition 3, in Section B) for a proof of (17). Essentially, λ is a constant depending on the network structure that globally takes into account and corrects for the selection and shrinkage properties the weights w_{ij} and r-stage adjacency have on the network time series.

The underlying GNAR structure points vectors in the direction of $(\mathbf{W} \odot \mathbf{S}_r + \mathbf{I_d})$ for which the magnitudes of the cross-covariances (i.e., the centered dot products) between $\boldsymbol{X}_{t+h}$ and $(\mathbf{W} \odot \mathbf{S}_r + \mathbf{I_d})\boldsymbol{X}_t$ are bounded by the magnitude of the autocovariance between independent components being projected onto the hypersphere $\{\boldsymbol{x} : \left\| \boldsymbol{x} - \overline{\boldsymbol{x}} \right\|_2 \leq (1 + \lambda)\}$.

By Theorem 2 and Section 4.2, decreasing r^* makes the model sparser and λ smaller, and the Corbit plot exploits this to highlight the lag and stage pairs at which the NACF cuts-off. Also, since the operator norm of $(\mathbf{W} \odot \mathbf{S}_r + \mathbf{I_d})$ is upper–bounded by $(1 + \lambda)$, the NACF highlights the (h, r) pairs at which the projected vectors point in the direction of the eigenvector associated to the largest eigenvalue of $(\mathbf{W} \odot \mathbf{S}_r + \mathbf{I_d})$, hence, the NACF is close to $pm1$ when the network weights and r-stage adjacency are such that the magnitude of projections compared in (17) are approximately the same. In that extreme case, future observations can be seen as eigenvectors of the network structure matrix $(\mathbf{W} \odot \mathbf{S}_r + \mathbf{I_d})$.

5 Modelling COVID–19 ventilation bed prevalence

Define the multivariate time series $\tilde{X}_{i,t}$ to be the recorded number of COVID–19 patients occupying mechanical ventilation beds for day t, for NHS Trust i, across $d = 140$ trusts in England. The $T = 452$ d-dimensional observations were obtained from the UK Government Coronavirus Dashboard (`coronavirus.data.gov.uk`) between April 2020 and July 2021. Patients who occupy mechanical ventilation beds are a subset of those COVID-positive patients who are, or become, seriously ill and require artificial ventilation. Some of these patients are directly transferred in on ventilation from other hospitals and care settings.

The $\tilde{X}_{i,t}$ observations are count data and it is not appropriate to use regular GNAR models directly and so, to stabilise variance and bring the data closer to normality, we study the well–known and understood transformed version: $X_{i,t} := \log(1 + \tilde{X}_{i,t})$. We stack the individual trust $X_{i,t}$ time series and denote $\boldsymbol{X}_t = (X_{1,t}, \cdots, X_{140,t})$, for $t = 1, \ldots, T = 452$.

In reality, there is no tangible single network connecting NHS Trusts. There are many ways a reasonable network could be constructed for modelling purposes and we outline one approach here. Our network was built using geographical 'as the crow flies' distances between NHS trusts. We define a D–connected network to be one where Trusts are directly connected, if they are less than D km apart. To find a good value of D we computed several D-connected networks with different values of $D > 0$. For each one we computed the residual sum of squares using a full fitted GNAR model, GNAR$(12, [4^{(12)}])$. The network that achieved the smallest residual sum of squares was with $D = 120$ km (approx 75 miles). A full GNAR model was used to capture any structure within a large possible number of lags and neighbour stages, any of which might be statistically significant in later model fitting with our chosen network (i.e., as we do not want to inadvertently rule out

detailed structure at this point). There are many reasonable networks that could be used instead, including those that delineate communications/transmission links more comprehensively. Our choice is intuitively attractive and can be seen to be a generalisation of partial correlation networks, see Epskamp and Fried (2018), for example.

The $X_{i,t}$ series for Trust i is associated with vertex i of our Trust network, which is depicted in Figure 1a. Our underlying assumption is that the behaviour of COVID-19 infection does not change drastically across location, and that the needs of similar hospitals can be described by the parsimonious GNAR model, which enables us to exploit the underlying structure. Hence, we propose modelling $\boldsymbol{X}_t$ as a stationary *global-*α GNAR process (4).

GNAR parsinomity allows us to use significantly more observations per parameter when estimating the autoregressive coefficients rather than separately for each node, as would be required for a (overparameterized) VAR model or even competitor CAR-like models . For instance, fitting a VAR(p) to $\boldsymbol{X}_t$ requires estimating (or, at the very least, having to consider) $p \times 140^2 = 19600 \times p$ unknown parameters, whereas, fitting a GNAR($p, [s_1, \ldots, s_p]$) requires estimating $p + \sum_{k=1}^{p} s_k$ parameters, which is upper–bounded by $p\,(1+6)$ given that the maximum r-stage per lag is six and we are modelling the data as a global–α GNAR process.

5.1 GNAR Model Selection

Using the ideas from Section 3, we focus on the correlation structure in $\{X_{i,t}\}$ and employ Corbit plots as graphical aids for assisting model selection. The observed NACF and PNACF values for our COVID-19 network time series are shown in Figures 4(a) and (b). Figure 4b shows that the partial network autocorrelation cut–offs after the first time lag and sharply decays after the first stage at the first time lag. It remains roughly constant at the first lag for stages larger than or equal to two at lag 1, and cuts-off sharply at all stages for all lags $h \geq 2$. Hence, our Corbit plot suggests looking at 1–lag models for which there does not appear to be a large contribution to autocorrelation from r-stage neighbours beyond the first stage. Looking at Corbit plots is considerably faster than a full evaluation of information criteria values such as AIC or BIC, as mentioned earlier.

We proceed by fitting a GNAR($1, [1]$) model and then compare it to GNAR($1, [6]$) and GNAR($6, [6^{(6)}]$) models, the latter being the one with the largest possible number of active r-stage regressions with the same number of lags. Table 1 compares results of different GNAR models by looking at one- and two-step predictive performance. For the two-step predictive performance each model is fitted to the first 447 observations of the COVID–19 network time series, and two–step prediction is performed by using the one-step prediction as a pseudo–observation. Table 1 shows that the order-6 model is the least–best choice based on one– and two-step predictive performance. The predictive errors for the remaining first order models are very similar with the GNAR($1, [6]$) best for one–step predictive error, very closely followed by the GNAR($1, [1]$) model, which is best for the two-step predictive performance, but there is little to choose between here. The AIC and BIC values are almost identical and, interestingly, select the model with the largest MSPE and number of parameters. However, the difference is less than 10% between the largest and smallest values for both criteria.

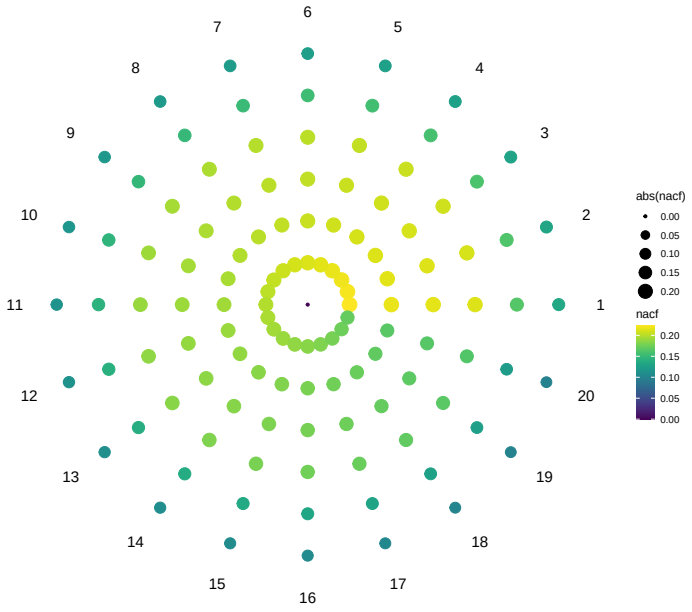

(a) COVID-19 series NACF Corbit plot.

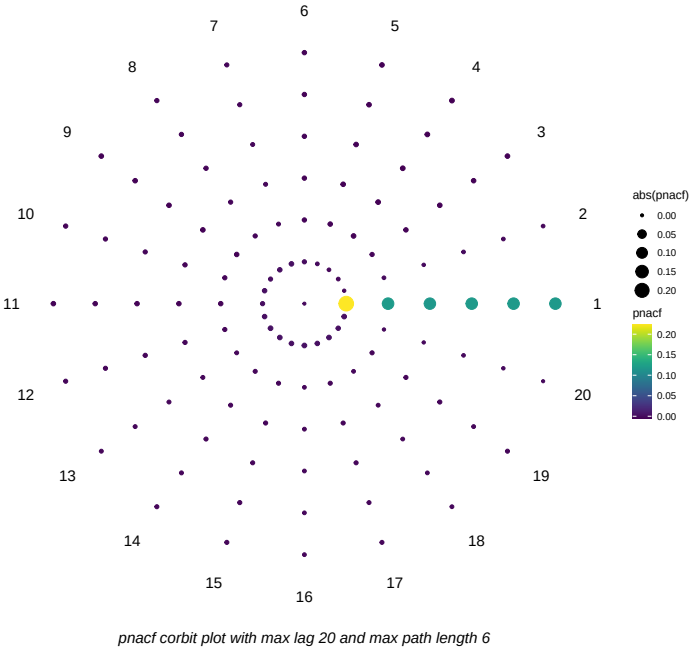

(b) COVID-19 series PNACF Corbit plot.

Figure 4: Corbit plots for (a) observed NACF, and (b) for observed PNACF with respect to the COVID-19 series; maximum lag is equal to 20 and maximum r-stage depth is equal to six. Plot (b) suggests a strong autoregressive behavior, which cuts-off after the first lag.

Model	AIC	BIC	One–step MSPE	Two–step MSPE
GNAR(1, [1])	-452.39	-452.37	5.09	8.81
GNAR(1, [6])	-452.53	-452.47	5.06	8.8
GNAR(6, [6, 6])	-467.35	-466.96	5.24	9.88

Table 1: AIC, BIC, One– and two–step mean–squared prediction error (MSPE) performance for different GNAR model order choices.

5.2 Comparison to Other Models

The underlying network structure aids not only in proposing a parsimonious GNAR model, it also permits estimation of the autoregressive coefficients more accurately and, we conjecture, reduces generalization error. In the interests of interpretability and illustration we select the GNAR$(1, [1])$ model and compare it to other

popular models. Table 2 compares the predictive performance of the GNAR$(1, [1])$ fit to VAR(1), sparse VAR(1), restricted VAR(1), decoupled AR(1) models, and to a conditional autoregressive first order temporal autoregressive (CARar) model, which is fitted using the `CARBayesST` package; see Lee et al. (2018) based on Rushworth et al. (2014). The comparison performs one–step prediction over the ten most recent times of the COVID–19 (network) time series. See the RMarkdown document (Section 3) for further details.

Model	MSPE(sd)	Mean No. Parameters
GNAR(1, [1])+	7.2(2.82)	2
GNAR(1, [1])	7.4(2.98)	2
CARar(1)	7.5(3.10)	4(+140)
Naive	7.6(3.12)	0
Res. VAR(1)	10.6(2.48)	3773
Sparse VAR(1)	11.4(2.80)	3089
VAR(1)	12.3(3.18)	19600
AR(1)	87.4(5.15)	140

Table 2: Mean number of parameters and one-step predictive performance for the COVID-19 (network) time series for five different time series models over ten predictions. The mean-squared prediction error (MSPE) standard deviation is shown within parenthesis. Naive is the observed value at the previous time step. GNAR$(1, [1])$+ denotes a GNAR$(1, [1])$ model estimated on centred data (i.e., subtracting column means before model fitting). The (+140) for the CARar model corresponds to the random effects in that model.

The models are fitted using the `GNAR` package (Knight et al., 2023) for the GNAR$(1, [1])$, `VARS` package (Pfaff, 2023) for fitting the VAR(1) and the restricted VAR(1), `forecast` package (Hyndman et al., 2023) for the 140 individual AR(1) models, and `sparsevar` (Vazzoler, 2021) for the Sparse VAR(1). We restricted each model to one lag for a fair comparison based on the autocorrelation analysis the Corbit plot in Figure 4b provides.

Table 2 shows that GNAR's MSPE is about 35% smaller than the nearest time series models Sparse VAR(1) and almost 30% smaller than restricted VAR(1). The centred GNAR is 4% better than CARar(1). In this particular situation CARar and GNAR are similar because CARar is structurally equivalent to a restricted GNAR with correlated er-

ror *limited to first stage neighbours*, but effectively having to also estimate $d = 140$ random effects 'pseudo–parameters'. However, it should be noted that CARar is significantly more computationally expensive than GNAR and much less flexible. We remark that CARar software does not provide functionality for forecasting, and so we created an *ad hoc* procedure that recasts the full Bayesian forecasting problem into a generalised least squares problem, where the correlated errors have the same covariance structure as the random effects. The forecasting performance of CARar using a full Bayesian method might be better or worse, but certainly enormously more computationally expensive, as it requires multiple code invocation equivalent to the parameter estimation, which is already expensive. See Appendix C in the supplementary material for details.

St. Ahead	GNAR(1, [1])	GNAR(1, [1])*	Res. VAR(1)	VAR(1)	Sp.VAR(1)
one	2.25	2.66	6.15	10.30	6.07
two	5.05	4.15	9.96	13.53	10.36
three	7.98	6.26	13.80	14.84	16.52

Table 3: Three-step ahead squared prediction error model comparison. GNAR$(1, [1])$ denotes global-α and GNAR$(1, [1])*$ denotes local-α. The realisation end point taken is $T = 300$, i.e., at the start of the second wave's peak. AR(1) were over 800 in all cases.

Table 3 shows one–, two– and three–step ahead comparisons for some of the methods described earlier but for an earlier end point at the start of the second wave's peak. It can be seen that GNAR reduces the mean squared prediction error by at least 40% in all cases. We did not include CARar as there is no forecasting functionality in the `CARBayesST` package, and we have not validated our *ad hoc* method further into the future.

Hence, for the right kind of data, i.e., those for which the GNAR model is (at least approximately) valid, then GNAR forecasting can be extremely competitive. Moreover, model parsinomity eases interpretation of the results: our analysis provides evidence that mechanical ventilation bed occupancies 'spreads' mostly through direct trust neighbours, and also on the previous number of beds occupied at the trust. The parameter estimates for the GNAR$(1, [1])$ were $\hat{\alpha}_1 \approx 0.95$ and $\hat{\beta}_{1,1} \approx 0.043$, and they were both statistically significant at the 0.1% level.

For completeness, we also tried fitting local–α models and predictive power improvement is negligible. The results are shown in the Appendices as Tables 7 to 16, where even with an extra 139 parameters the improvement in predictive error is never more than 3%, often nearer 1 or 2%, and in two cases out of the ten tables the simpler GNAR does better. This modelling exercise provides further validation for our initial global–α choice.

5.3 Model Interpretation and Analysis

Another attractive property of GNAR models is that they can handle missing data and zero-values by weight readjustment; see Knight et al. (2020). We extend this idea to study the correlation structure of the two main COVID–19 outbreaks in England, the first outbreak was from April 2020 to July 2020 and the second one was from September 2020 to July 2021. We visualise the differences in the correlation structure during these different time periods by looking at R–Corbit plots, such as the one for NACF in Figure 5, the equivalent plot for PNACF is shown in Figure 8 in the Appendix.

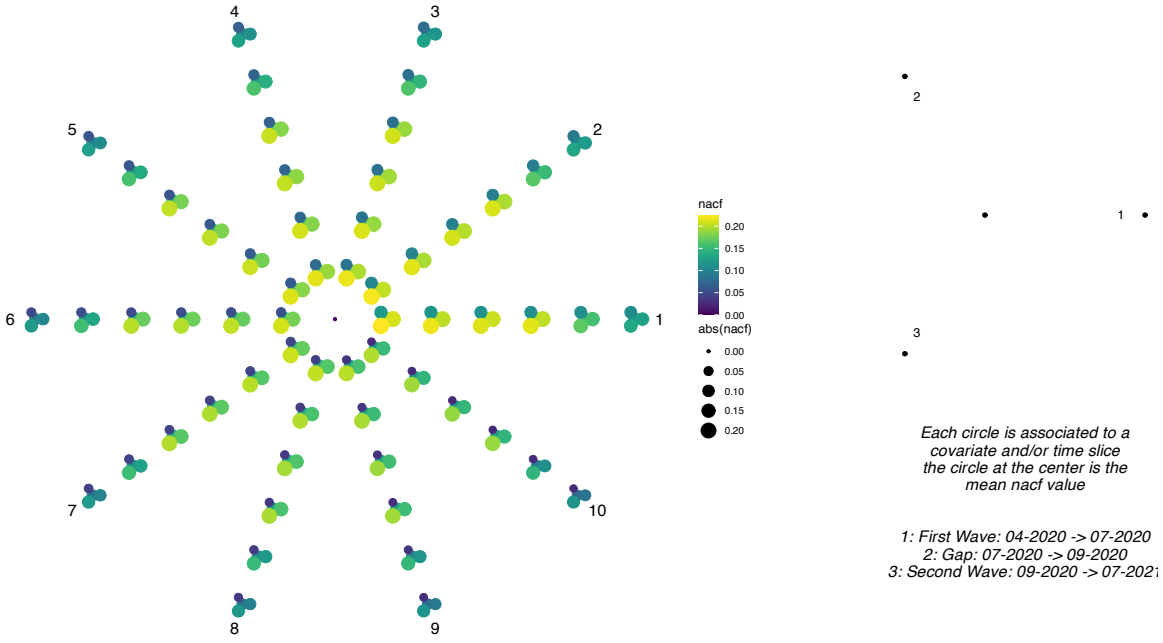

Figure 5: COVID–19 series NACF R-Corbit plot. The plot compares the NACF values between the two COVID-19 outbreaks and the gap between them. The maximum lag is ten and the maximum r-stage depth is equal to six. See text for description.

R–Corbit plots allow us to compare the NACF and PNACF values for different time-slices and/or covariates, we read the plot in the same manner as the Corbit plot and look at the legend on the right–hand side for distinguishing between covariates and/or time–slices. The point at the centre is the mean value of the NACF or PNACF values arising from the time–slices and/or covariate data splits. Essentially, if $c \in \{1, \ldots, C\}$, where $C \in \mathbb{N}$ is the number of levels in the covariate or time-slices, then the value at the centre is $\text{nacf}(h, r) = C^{-1} \sum_{c=1}^{C} \text{nacf}_c(h, r)$, where $\text{nacf}_c(h, r)$ is the NACF value corresponding to covariate–level/time–slice c.

The R–Corbit plot in Figure 5 suggests that the correlation structure is different between the three time-slices, largest for the second outbreak and smallest for the gap. The gap period of July 2020 to September 2020 is characterised by constantly zero-valued observations for many Trusts (but not all of them), which, in the full–data models above, contribute to the overall variance, but not to the non–zero lag/stage correlations and related parameters and perhaps making them appear smaller than would be the case should the two main waves be analysed separately.

We focus on model comparisons for the second outbreak in the table below. Prediction error is calculated using the last five realisations as test observations for the model fitted using the rest of the data.

Model	Mean-squared Prediction Error One-Step	Two-Step	No. Parameters	Sig. Parameters
GNAR(1, [1])	5.43	12.74	2	2
GNAR(1, [6])	5.46	12.73	7	7
GNAR(6, $[6^{(6)}]$)	5.87	12.99	42	20

Table 4: Comparison of different GNAR model orders for the series corresponding to the number of mechanical ventilation beds needed during the second COVID-19 wave for hospital trusts in the network shown by Figure 1a.

Table 4 reflects the information that the Corbit plots in Figure 4 provide by noting that models with more than one lag should be discarded based on prediction error and the number of statistically significant parameters at the 1% level. Moreover, it shows the slight performance improvements increasing r^* from one to six has. Therefore, we, as previously, select GNAR(1, [1]), and exploit the ideas in Section 4 by introducing the following measures of relevance.

5.4 Node Relevance

Once we fix an estimate of r^*, we can find the sparse weight matrix $\mathbf{W} \odot \mathbf{S}_{(r^*)}$, where $\mathbf{S}_{(r^*)} = \sum_{r=1}^{r^*} \mathbf{S}_r$, from which it is possible to compare the relevance each node has. Motivated by (17) we define the global relevance index as

$$\text{globindex}(X_{i,t}) := \left(\sum_{j=1}^{d} [\mathbf{W} \odot \mathbf{S}_{(r^*)}]_{ji} \right) \left\{ \max_{l \in \mathcal{K}} \left(\sum_{j=1}^{d} [\mathbf{W} \odot \mathbf{S}_{(r^*)}]_{jl} \right) \right\}^{-1}, \tag{18}$$

which computes the ratio between the largest column sum for active nodes and a particular node. We interpret this as the relevance each node has globally on the correlation structure.

Next, we define a measure of the strength of pairwise interactions as the weighted contribution from all estimated $\hat{\beta}_{kr}$ across active stages (i.e., $1 \leq r \leq r^*$), formally,

$$\text{local}_i(j) := \left(w_{ij} \sum_{k=1}^{p} |\hat{\beta}_{kr}| \right) \left\{ \sum_{l \in \mathcal{N}(i)} \sum_{r=1}^{r^*} \sum_{k=1}^{p} w_{il} |\hat{\beta}_{kr}| \right) \right\}^{-1}, \tag{19}$$

where $\mathcal{N}(i) = \cup_{r=1}^{r^*} \mathcal{N}_r(i)$, and i and j can only be r-stage neighbours for one r. Note that this results in w_{ij} if we restrict the above to a specific r-stage. This index is larger as w_{ij} gets closer to one. Hence, the index computes the percentage of the neighbourhood coefficient across all lags corresponding to the specific pair (i.e., how strong, relative to other active nodes, j is for forecasting i). Thence, $\text{local}_i(j)$ is not a symmetric function of i and j.

Also, by Theorem 2, we can plot the correlation structure of our selected model based on the distances in the underlying network, which we plot by distinguishing between active nodes: $\delta(i,j) \leq r^*$, colliding nodes: $r^* < \delta(i,j) \leq 2r^*$ and conditionally uncorrelated nodes: $\delta(i,j) \geq 2r^*+1$. Formally, we can also compute the relative strength of conditionally correlated nodes as

$$\text{rscc}(i,j) := \mathbb{I}\{\delta(i,j) \leq r^*\}\{\delta(i,j)\}^{-1} + \mathbb{I}\{r^* < \delta(i,j) \leq 2r^*\}\{2\delta(i,j)\}^{-1}, \tag{20}$$

where the distances are computed on the underlying network, and we divide by two the distance for nodes that are conditionally correlated despite not being active in their respective neighbourhood regressions.

These measures of global relevance, $\text{globindex}(X_{i,t})$ and local relevance, $\text{local}_i(j)$, are shown in detail in Appendix D. Below, we plot a coloured version of the NHS network, where colours are assigned using the values of $\text{globindex}(X_{i,t})$ as given by (18) for $r^* = 1$. We remark that these diagnostic statistics depend on the time series values through the choice of r^* and maximum lag, as well as on network connectivity and edge weights.

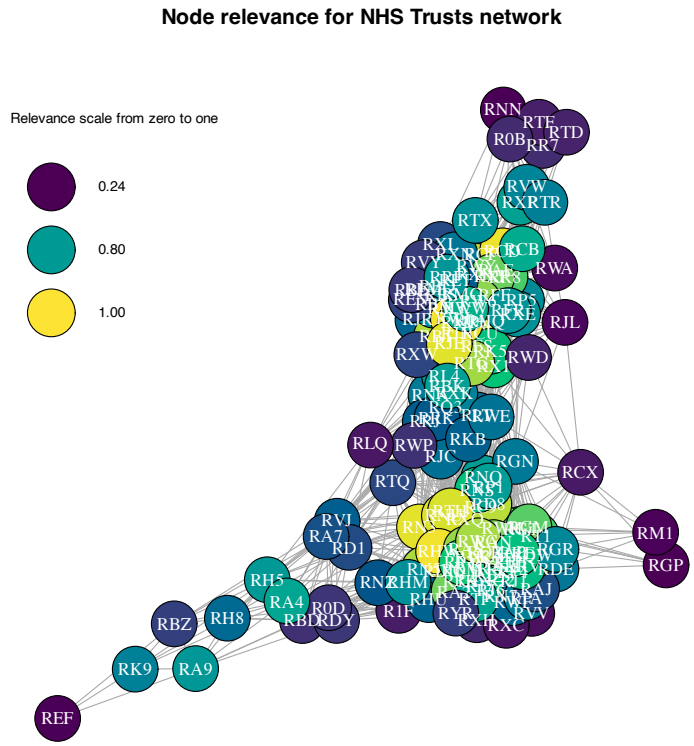

Figure 6: NHS Trusts network coloured by global node relevance values, i.e., $\text{globindex}(X_{i,t})$ given by (18) for $r^* = 1$. Nodes that have a larger effect on network autocorrelation are brighter (yellow) and less relevant ones darker (violet). See the RMarkdown document mentioned in the Conclusion (link provided in the Appendix) for $r^* = 3$ and $r^* = 6$, and Figure 14 in Appendix D for a full page size version of this plot.

Figure 6 shows the $\text{globindex}(X_{i,t})$ values for all NHS Trusts. Individual Trust identities are hard to discern from this plot, but it is instructive to examine them in a bit more detail. The top ten Trusts for $\text{globindex}(X_{i,t})$ in decreasing order are 1. Buckinghamshire, 2. East Cheshire, 3. Stockport, 4. Royal Berkshire, 5. Harrogate District, 6. Tameside Glossop, 7. Great Western (Swindon), 8. University Hospitals of North Midlands, 9. Oxford Health and 10. Oxford University Hospitals with globindex relevance ranging from 1.000 to 0.952. Figure 7 shows the most relevant $\text{globindex}(X_{i,t})$ Trusts for both the first ten and first

sixty Trusts in decreasing order. It is interesting that the most relevant Trusts relating to the network time series dynamics are located in two clear clusters: one positioned to the north-west of London (between London, the West Midlands [Birmingham], Bristol and the Southampton/Portsmouth urban centres) and the other between and around the urban centres of the West Midlands [Birmingham], Manchester, Sheffield, Nottingham, West Yorkshire and Liverpool. It is noticeable that in the top ten globindex($X_{i,t}$) relevance list there are *no* Trusts in urban centres and *only* eighteen in the top sixty list. From the point of view of network time series dynamics, the most relevant trusts are not urban centres *per se*, but intermediately-located Trusts. Having said this, it is intriguing that there do not seem to be relevant Trusts immediately to the south and east of Birmingham, nor between Yorkshire and Tyneside, nor in the densely populated area south and east of London. The location of these relevant Trusts might have implications for future epidemic mitigation that could be taken to minimise viral spread.

For example, rather than national or regional lockdown the aim would be to impede movement between areas as a firebreak. Such a firebreak is a larger, regional, version of, e.g., firebreak culls that existed as a control measure during the 2001 foot–and–mouth epidemic (Haydon et al., 2004) and part of the current foot–and–mouth control strategy for Great Britain, see DEFRA (2011).

Knowledge of such relevant locations might enable a more targeted and efficient set of restrictions to be implemented, rather than a blanket approach, which imposes costs on unafflicted areas. Obviously, such mitigations require further investigation and research.

The least relevant globindex($X_{i,t}$) Trusts are those in the extremities of the network, typically coastal towns, and are shown as black squares in Figure 7 (the exception being the Wye Valley NHS Trust, which is an extremity of the English NHS Trust network on the border with Wales). That the least relevant Trusts are located at network extremities is perhaps not surprising as there are no susceptibles located in the sea and the epidemic can only be reflected back to the region(s) that initially 'infected' the least relevant regions.

Figure 11 in Appendix D shows neighbourhood regressions sparseness by highlighting the strength of pairwise neighbourhood regression coefficients measured by $\text{local}_i(j)$ in (19) for NHS Trust REF (located in Cornwall). Looking at similar plots of local relevance for different nodes suggests that effects of one–stage neighbours are evenly spread, which highlights parsimonious properties of GNAR models. Further, it appears that Trusts connected to many one-stage neighbours behave in a group–like manner, i.e., there is no single node that appears to be more relevant. Whereas, if a Trust is in a more isolated community, e.g., nodes corresponding to Trusts in Cornwall, then the Trust is affected more by each of its one-stage neighbours. The largest (yellow) coefficient on the right-hand side of the plot corresponds to transmission from the University Hospitals Plymouth to the Royal Cornwall Hospitals NHS Trusts, which can be thought of as the main conduit town into Cornwall. Thus, the plot suggests, unsurprisingly, that communities at the network's edge have different characteristics than the ones closer to the main population centres.

5.5 Discussion

An attractive property of GNAR parsinomity is that it enables us to interpret a large number of interactions with a relatively small number of parameters, in our case we can interpret the interactions between 140 NHS trusts with just two parameters and *still* have

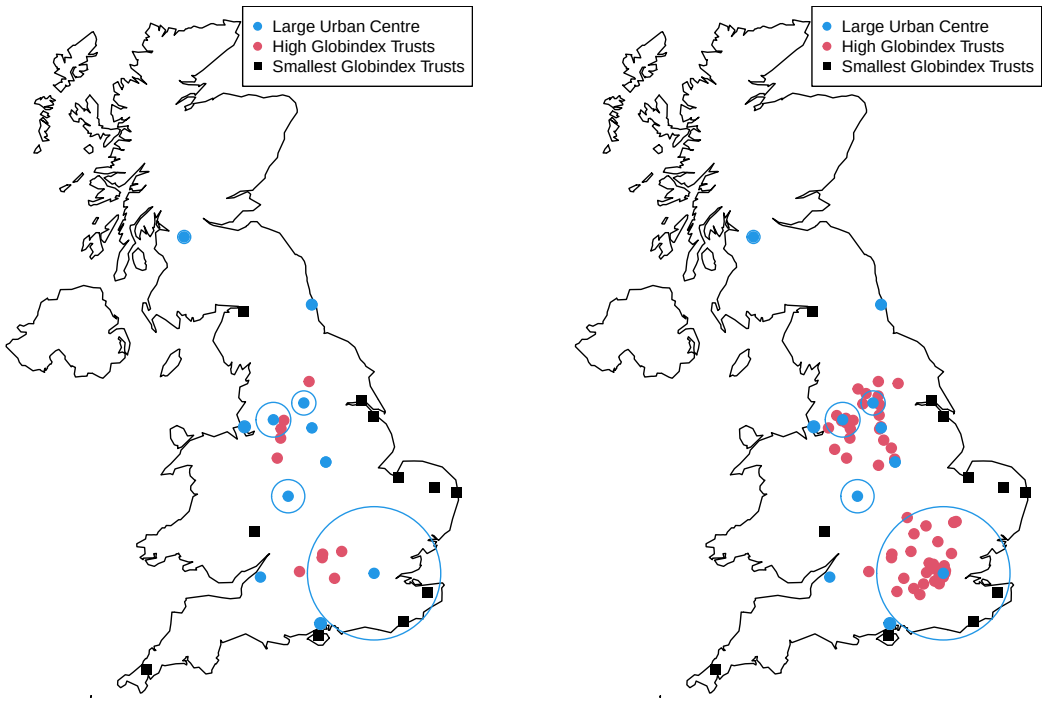

(a) (b)

Figure 7: Blue dots show top eleven urban centres in the UK. Blue circles indicate urban centre population size with London as approximately 9.78 million people. Black squares are ten least 'relevant' globindex($X_{i,t}$) Trusts. Red dots: highest relevant NHS Trusts according to globindex($X_{i,t}$). (a) top ten globindex($X_{i,t}$) Trust locations (b) top sixty globindex($X_{i,t}$) Trust locations.

superior forecasting performance, as shown by Table 1. The Corbit plots in Figure 4 show the strong autoregressive structure of the series $\boldsymbol{X}_t$, highlighting that correlation cuts-off after lag one.

Our chosen model is a global–α GNAR$(1,[1])$, which mandates that the expected value for each node is a linear combination of its value at time lag one (with coefficient $\hat{\alpha}_1 \approx= 0.95$ from Section 5.2) and its 1–stage neighbours at time lag one (with coefficient $\hat{\beta}_{1,1} \approx 0.043$). The transfer from the same trust at the previous time step at 0.95 is considerably larger than the 0.043 neighbor contribution, but there are typically many neighbors, making the neighbour contribution non–neglible.

Further, the expected number of beds at trust i at time t increases, if either the number of beds at trust i increases at time $t-1$ and/or the number of transfers at its 1-stage neighbours increases at $t-1$. Hence, the outbreak acts in a 'continuous' matter, i.e., bed demand spreads between 1-stage neighbours. Crucially, we concluded that demand does not spread via from higher-stage neighbours and we inferred this as a result of *statistical model selection*, not by an *a priori* assumption, as is implicitly, and perhaps unthinkingly in some simpler network time series and conditional autoregressive models.

Relating to our discussion on mitigations earlier, if local communities can block the spread to 1–stage neighbours of their 1–stage neighbours (i.e., their 2–stage neighbours), then, on average, this would also create a firewall between them and other communities in the network. This obvious–sounding statement is encapsulated by Theorem 2, which reflects this by noting that two nodes are uncorrelated at all lags given their 2–stage neighbours, i.e., the outbreak cannot jump between nodes separated by at least two edges. It must travel through each nodes 1–stage neighbours.

Further, and interestingly, the R–Corbit plot in Figure 5 shows that there is an increase in correlation during the second outbreak, which we attribute to less stringent measures and an increase in the number of interactions between nodes (i.e., more people travelling across different areas of England); see Mathieu et al. (2022). These results reflect the node relevance in Figure 6, which shows that the nodes with the most relevance are close to London, and that the less relevant nodes are at the extremities, e.g., NHS Trust REF, i.e., Royal Cornwall Hospitals NHS Trusts. Nevertheless, all nodes are similarly important given that we constrain the model to 1-stage neighbourhood regression, which shows the global properties of how demand for mechanical ventilation beds due to COVID–19 cases spread throughout England during the pandemic.

6 Conclusion and Further Work

We have introduced new methods for modelling and inferring relationships present in network time series. Section 2 reviewed the GNAR model introduced by Knight et al. (2016, 2020) and presents a new compact hierarchical matrix representation, which is easier to manipulate. Subsequently, we proposed the NACF and the PNACF as diagnostic statistics, which can be visualised with Corbit plots. These choices for measuring correlation are not the only possible ones, however, their usefulness and ease of interpretation as graphical aids for model selection are illustrated in Section 5. Moreover, the ideas in Section 4 show the connection between GNAR models and graphical models, which suggest a clear interpretation of the relationship between nodes depending on their distance on the graph,

and how this affects conditional correlation; see Theorem 2. Also, we exhibit a possible interpretation of GNAR models as a constrained VAR that exploits prior knowledge of the network for performing variable selection and shrinkage, which enables us to study the connection between model constraints, prior information and parameter updates. These ideas allow us to study the local interactions between nodes, and the properties of the network as a composite object. Further, it exhibits how we can extend results from VAR theory to the GNAR framework by properly adjusting the correspondence between VAR parametrizations and GNAR formulations.

We remark that the GNAR framework is useful for specific problems where the data can be properly described by an underlying network, which induces a particular correlation structure. Section 5 shows the advantages GNAR methods have when studying problems similar to the demand for mechanical ventilation beds during the COVID–19 pandemic. Also, motivated by Section 4.2, investigating the connection between prior information and posterior distributions, such as assigning a prior to the association function between nodes might improve forecasting performance and complex models' interpretability. Future work could focus on trend removal and tests of stationarity. Also, a more thorough analysis of the NACF and PNACF might reveal interesting statistical properties for model selection, and aid in the study of AIC and BIC as criteria for parsimonious model selection; see Akaike (1973); Schwarz (1978).

Another area for future exploration is that of the construction of the underlying network. We believe our current method is sensible, but it is not the only possibility. A more refined local geographically-derived network might be preferable such as one that takes into account key transport connections. For example, some Trusts further apart than our 120 km might be strongly connected by a commuter rail line or they are a regional centre, perhaps, for some kinds of healthcare from quite a large region. We also considered more general mathematical tessellations, such as Dirichlet, but these suffer from the 'long thin triangle' issue, which connects infeasibly far apart Trusts, such as on the Wirral and Devon in north-west and south-west England, respectively, and hence are not really viable for our problem. A potential issue is that we use the data several times for different purposes: to select the $D = 120$ km distance limit to connect NHS Trusts, to compute and assess models using NACF/PNACF and predictive inference (properly using out-of-sample forecasts). Further work is necessary to understand whether this 'multiple-dipping' of the data is acceptable, whether it affects reliability, and it might be preferable to investigate and implement methods of post-selective inference such as splitting strategies, see, e.g. García Rasines and Young (2023).

Essentially, GNAR is a parsimonious model that enables us to estimate fewer parameters more efficiently and precisely, even in high-dimensional settings. Furthermore, it is more transparent than overparametrized VAR, which facilitates interpretation and replication. The code for our plots and NACF/PNACF functions are incorporated into the CRAN `GNAR` package. Many further examples and material relating to our work can be found in an RMarkdown document (link provided in the supplementary material).

The UK Covid–19 enquiry (`https://covid19.public-inquiry.uk/`) highlights the importance of analysing all aspects of the pandemic. The enquiry's remit specifically relates to "the state of the UK's central structures and procedures for pandemic emergency preparedness, resilience and response". Statistical modelling of complex health services data has an important role to play in this crucial initiative.

Acknowledgments

We gratefully acknowledge the following support: Nason from EPSRC NeST Programme grant EP/X002195/1; Salnikov from the UCL Great Ormond Street Institute of Child Health, NeST contribution from Imperial College London, the Great Ormond Street Hospital DRIVE Informatics Programme, and the Bank of Mexico. Cortina–Borja supported by the NIHR Great Ormond Street Hospital Biomedical Research Centre. The views expressed are those of the authors and not necessarily those of the EPSRC, National Health Service (NHS), the NIHR or the UK Department of Health.

SUPPLEMENTARY MATERIAL IN APPENDICES

A: Model Predictions Tables of model prediction results.

B: Further plots Corbit plot with dashed line separating lag zero from highest lag. Rectangular Corbit plots.

C: CARar and GNAR Detailed comparison and notes.

SUPPLEMENTARY MATERIAL IN SEPARATE DOCUMENT

Correlation Structure Proof: Proof and illustration of Theorem 2. (PDF/LaTeX)

Network Autocorrelation Function Properties: Derivation and properties of the NACF given by Definition 3. (PDF/LaTeX)

Algorithms and Properties of r-stage Adjacency Matrices: Brief document exhibiting the properties and possible computation techniques for r-stage adjacency matrices given by Definition 1. (PDF/LaTeX)

R-package for Graphical Aids routine: R-package **GNAR** and scripts containing code to perform the diagnostic methods described in the article. The package also contains all data sets used as examples in the article. (GNU zipped tar file). The GNAR package can be accessed HERE. Further examples, further details on some of the paper's examples and some new examples are presented in the following RMarkdown document: R Markdown link: click here.

COVID-19 Series data set: Data set analysed in Section 5. The data set is available in the `GNAR` package, the file is `logMVbedMVC.vts`. A help file contains a detailed description of the data set and how it was obtained from the UK Government Coronavirus Dashboard (`coronavirus.data.gov.uk`) between April 2020 and July 2021.

A Model Predictions

We perform one-step prediction ten times to have a more robust estimate of out-of-sample prediction error, the summarised results are shown below.

Model	MSE(sd)	Mean No. Parameters
GNAR(1, [1])	7.414(2.977)	2
Sparse VAR(1)	11.307(2.768)	2962
Res. VAR(1)	10.614(2.482)	3767
VAR(1)	12.275(3.184)	19600
AR(1)	87.402(5.146)	140
GNAR(1, [1])*	7.313(2.900)	141

Table 5: One-step predictive performance and average number of parameters for the COVID-19 (network) time series for five different time series models. The MSE standard deviation is shown within parenthesis. GNAR(1, [1])* uses a different α_{id} for every NHS trust.

One-step prediction error (i.e., $||\hat{\boldsymbol{X}}_t - \boldsymbol{X}_t||^2$) comparison between model predictions and the known test values. We perform the experiment ten times for $t = 443, \ldots, 452$, and show the standard deviation within parenthesis next to each MSE value. The third column indicates the average number of active (i.e., non-zero coefficients) each model has throughout the experiment.

Interestingly, GNAR parsinomity not only results in the smallest one-step prediction error in this case, it also has the smallest variance and standard deviation. Moreover, it is possible to fit more complex GNAR models since the number of unknown parameters is drastically smaller than for the other models, most notably, fitting a GNAR(1, [1]) requires estimating two parameters, whereas sparse VAR(1) requires estimating, on average, 3061 coefficients.

Remarkably, GNAR(1, [1]) accomplishes a smaller squared prediction error than sparse VAR(1) does with much fewer parameters.

A.1 Model Comparison for one-lag differenced series

Model	MSE	Mean Active Parameters
GNAR(1, 1)	7.847(2.908)	2
Sparse VAR(1)	7.686(2.940)	451
Res. VAR(1)	9.149(3.068)	1840
VAR(1)	11.371(3.525)	19600
AR(1)	7.816(2.931)	140

Table 6: Mean number of parameters and one-step predictive performance for the differenced COVID-19 (network) time series for five different time series models. The MSE standard deviation is shown within parenthesis.

A.2 Prediction Error Tables for the Ten Experiments

Below are the prediction error tables for each of the test points $\boldsymbol{X}_t$, where $t = 443, \ldots, 452$, and GNAR(1, [1])* uses a different α_{id} for every NHS trust.

Model	Active Parameters	One-Step SPE
GNAR(1, [1])	2	5.441
VAR(1)	140^2	11.613
Res. VAR(1)	3821	9.902
Sparse VAR(1)	2980	10.212
AR(1)	140	82.055
GNAR(1, [1])*	141	5.324

Table 7: One-step prediction error, $\hat{\boldsymbol{X}}_{443}$ is predicted using the previous 442 observations.

Model	Active Parameters	One-Step SPE
GNAR(1, [1])	2	7.86
VAR(1)	140^2	12.804
Res. VAR(1)	3712	11.504
Sparse VAR(1)	2992	11.533
AR(1)	140	78.748
GNAR(1, [1])*	141	7.833

Table 8: One-step prediction error, $\hat{\boldsymbol{X}}_{444}$ is predicted using the previous 443 observations.

Model	Active Parameters	One-Step SPE
GNAR(1, [1])	2	10.286
VAR(1)	140^2	12.52
Res. VAR(1)	3730	11.605
Sparse VAR(1)	2785	12.986
AR(1)	140	82.571
GNAR(1, [1])*	141	10.173

Table 9: One-step prediction error, $\hat{\boldsymbol{X}}_{445}$ is predicted using the previous 444 observations.

Model	Active Parameters	One-Step SPE
GNAR(1, [1])	2	12.953
VAR(1)	140^2	17.762
Res. VAR(1)	3812	14.472
Sparse VAR(1)	3283	15.057
AR(1)	140	86.781
GNAR(1, [1])*	141	12.676

Table 10: One-step prediction error, $\hat{\boldsymbol{X}}_{446}$ is predicted using the previous 455 observations.

Model	Active Parameters	One-Step SPE
GNAR(1, [1])	2	7.525
VAR(1)	140^2	13.82
Res. VAR(1)	3761	10.815
Sparse VAR(1)	3315	11.995
AR(1)	140	89.097
GNAR(1, [1])*	141	7.431

Table 11: One-step prediction error, $\hat{\boldsymbol{X}}_{447}$ is predicted using the previous 446 observations.

Model	Active Parameters	One-Step SPE
GNAR(1, [1])	2	5.088
VAR(1)	140^2	12.504
Res. VAR(1)	3830	9.976
Sparse VAR(1)	3609	10.169
AR(1)	140	88.181
GNAR(1, [1])*	141	4.989

Table 12: One-step prediction error, $\hat{\boldsymbol{X}}_{448}$ is predicted using the previous 447 observations.

Model	Active Parameters	One-Step SPE
GNAR(1, [1])	2	4.44
VAR(1)	140^2	7.978
Res. VAR(1)	3738	7.716
Sparse VAR(1)	3030	7.918
AR(1)	140	91.004
GNAR(1, [1])*	141	4.466

Table 13: One-step prediction error, $\hat{\boldsymbol{X}}_{449}$ is predicted using the previous 448 observations.

Model	Active Parameters	One-Step SPE
GNAR(1, [1])	2	3.061
VAR(1)	140^2	7.196
Res. VAR(1)	3759	5.888
Sparse VAR(1)	3017	6.842
AR(1)	140	88.066
GNAR(1, [1])*	141	3.089

Table 14: One-step prediction error, $\hat{\boldsymbol{X}}_{450}$ is predicted using the previous 449 observations.

Model	Active Parameters	One-Step SPE
GNAR(1, [1])	2	8.868
VAR(1)	140^2	10.869
Res. VAR(1)	3772	10.999
Sparse VAR(1)	3016	11.68
AR(1)	140	91.151
GNAR(1, [1])*	141	8.607

Table 15: One-step prediction error, $\hat{\boldsymbol{X}}_{451}$ is predicted using the previous 450 observations.

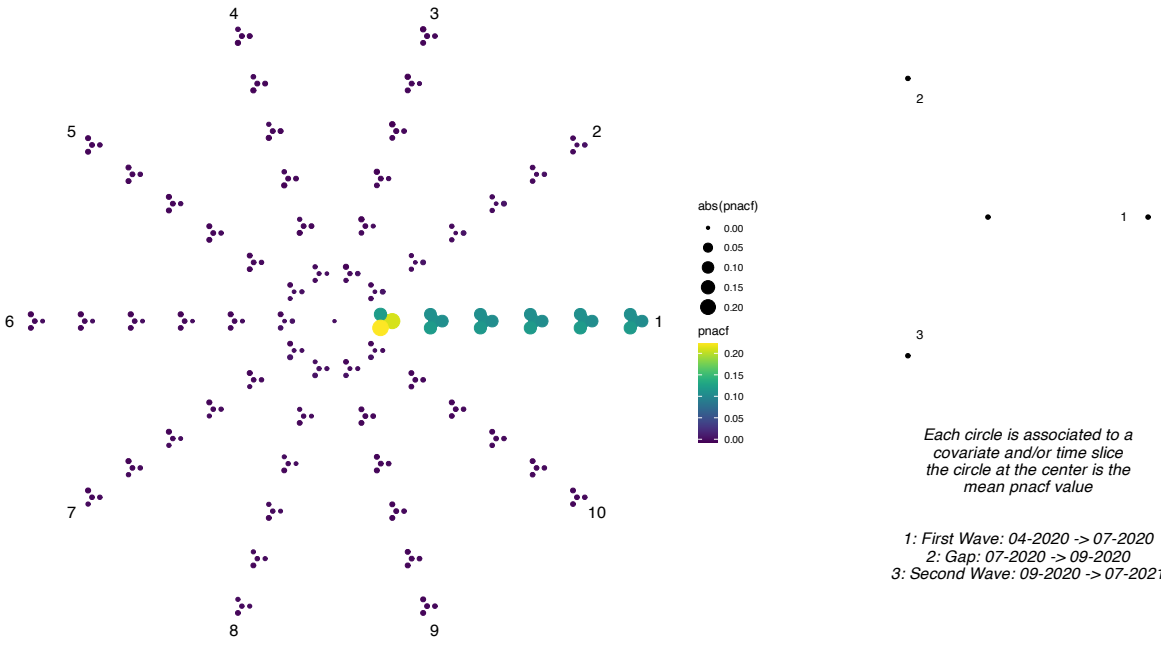

Figure 8: COVID-19 series PNACF R-Corbit plot. The plot compares the PNACF values between the two COVID-19 outbreaks and the gap between them. The maximum lag is ten and the maximum r-stage depth is equal to six. See Section 5.3 for description.

Model	Active Parameters	One-Step SPE
GNAR(1, [1])	2	8.623
VAR(1)	140^2	15.693
Res. VAR(1)	3794	13.258
Sparse VAR(1)	3299	15.715
AR(1)	140	96.361
GNAR(1, [1])*	141	8.546

Table 16: One-step prediction error, $\hat{\boldsymbol{X}}_{452}$ is predicted using the previous 451 observations.

B Further Plots, Alternatives and Options

B.1 R-Corbit plot

Figure 8 shows the PNACF R-Corbit plot referred to in the text above in Section 5.3.

B.2 Corbit plot with 'line gap'

Figure 9 shows a Corbit plot with a 'line gap'. This reflects the fact that lag 1 and lag 20 are not actually close, so a dotted line is drawn to indicate that lag 20 is the last and highest lag and that the next lag in the circle (lag 1) is not a continuation. Producing this is an option in the software and is the result of a suggestion of Professor Berthold Lausen, University of Essex.

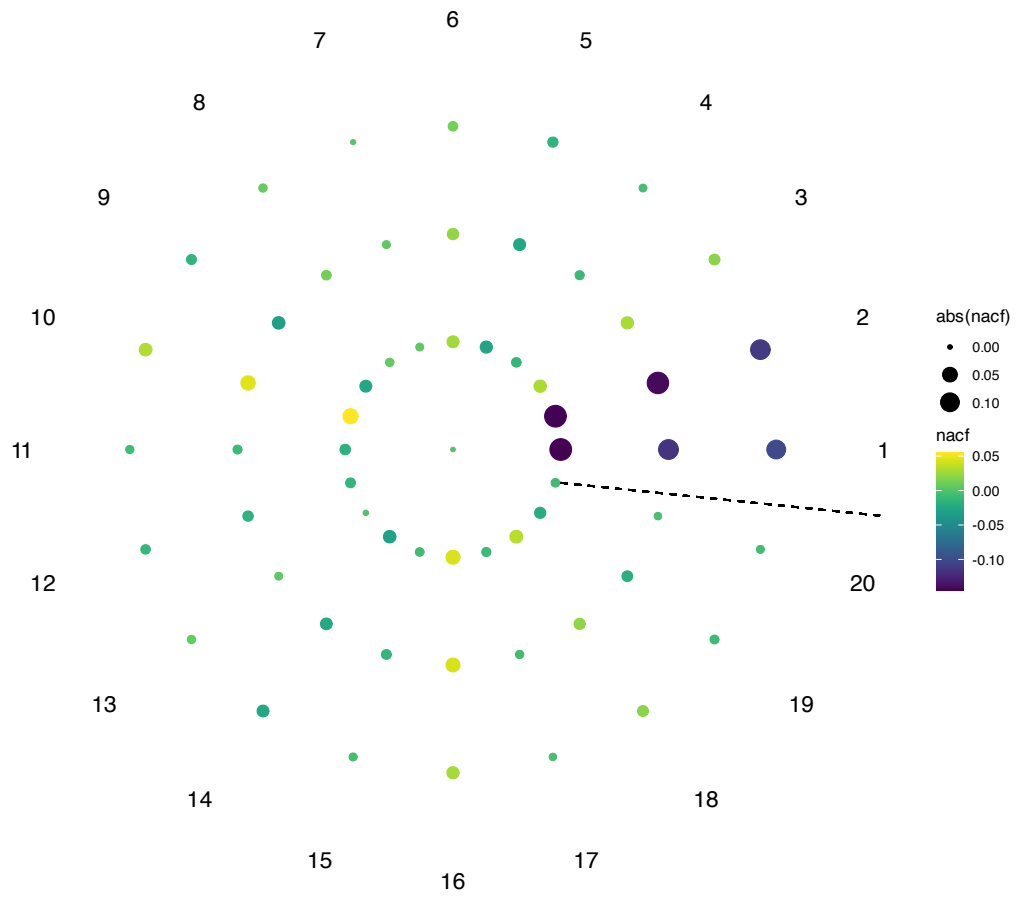

nacf Corbit plot with max lag 20 and max path length 3

Figure 9: NACF Corbit plot of the **gdpVTS** (included in the `GNAR` package). The plot includes the optional *line gap* argument, which highlights that lags are not a periodic quantity, and separates the first and last lags across all r-stages explicitly.

B.3 Rectangular Corbit plots

It is possible to format the NACF and PNACF in rectangular form, which might be more comfortable for some users. Figures 10 is the rectangular version of the GNAR$(2, [1, 1])$ simulation whose Corbit plot is shown in Figure 2 of the main article. Producing the rectangular versions is an option in the software.

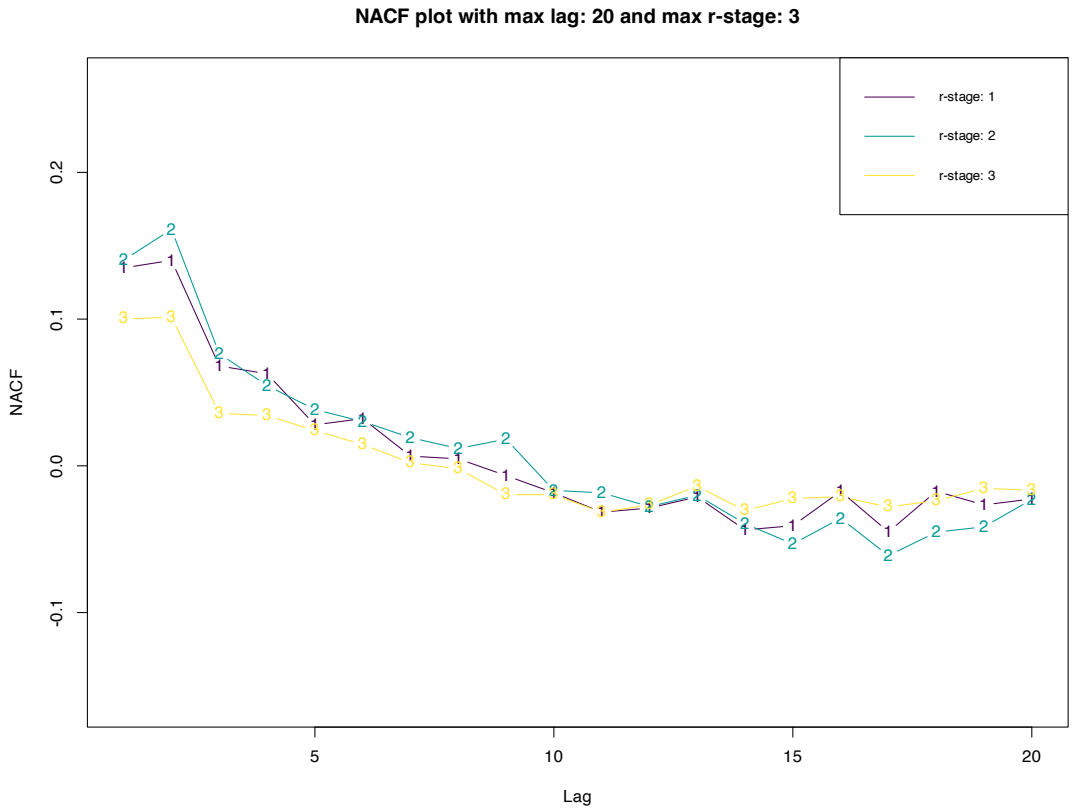

Figure 10: Rectangular NACF plot.

C CARar and GNAR comparison

We are interested in modelling data that can be described as either a network time series, i.e., $\mathcal{X} = (\boldsymbol{X}_t, \mathcal{G})$, or as a spatio-temporal process characterised by a parsimonious covariance structure. In this document, we compare a conditional autoregressive temporal autoregressive (CARar) model to a global-α generalised network autoregressive (GNAR) model. Both models assume knowledge of an underlying adjacency structure, in the case of GNAR it is the network's adjacency matrix, whereas, for CARar it is the neighbourhood adjacency matrix for areal unit data. We will use the following notation:

- $\mathcal{K} := [d] = \{1, \ldots, d\}$, set of nodes, i.e., dimension of the multivariate process.
- $\mathcal{E} \subseteq \mathcal{K} \times \mathcal{K}$, edge set, i.e., if $(i, j) \in \mathcal{E}$, then there is an edge between nodes i and j.
- $\mathcal{G} := (\mathcal{K}, \mathcal{E})$ underlying network structure of the process, e.g., land borders between counties.
- $\boldsymbol{X}_t$: a multivariate time series of dimension d, such that each univariate time series $X_{i,t}$ is linked to node i in the network $\mathcal{G}$.
- $\mathbf{S}_r$: the r-stage adjancency matrix of $\mathcal{G}$, i.e., $[\mathbf{S}_r]_{ij} = \mathbb{I}\{d(i, j) = r\}$, where $\mathbb{I}$ is the indicator function and $d(i, j)$ is the shortest path between nodes i and j in $\mathcal{G}$.

- $\mathbf{W}$: the weights matrix for network $\mathcal{G}$, i.e., $[\mathbf{W}]_{ij} = w_{ij} \in [0,1]$ is the weight between nodes i and j, e.g., $1/(\sum_{\ell=1}^{d}[\mathbf{S}_r]_{i\ell})$.
- $\mathbf{\Sigma_u}$: covariance matrix of the d-dimensional residual process $\boldsymbol{u}_t$.
- $\alpha_k \in \mathbb{R}$ autoregressive coefficient at the kth lag, $\beta_{kr} \in \mathbb{R}$ neighbourhood regression coefficient at network distance r and kth lag.

C.1 CAR model

CARar models are hierarchical models that describe spatio-temporal interactions based on a neighbourhood structure for random effects, the model is given by

$$
\begin{aligned}
&X_{i,t} = \mu + \phi_{i,t} + u_{i,t} \\
&\boldsymbol{\phi}_t | \boldsymbol{\phi}_{t-1} \sim \mathrm{N}(\rho\boldsymbol{\phi}_{t-1}, \tau^2\mathbf{Q}^{-1}) \\
&\mathbf{Q} = \xi\left\{\mathrm{diag}\left(\sum_{j=1}^{d}[\mathbf{S}_1]_{ij}\right) - \mathbf{S}_1\right\} + (1-\xi)\mathbf{I_d} \\
&\tau^2 \sim \mathrm{inverseGamma}(a,b) \\
&\rho, \xi \sim \mathrm{Unif}(0,1),
\end{aligned}
$$

where $\mathbf{I_d}$ is the $d \times d$ identity matrix, $u_{i,t} \sim \mathrm{N}(0, \sigma_u^2)$ at all times t is independent of μ and $\phi_{i,t}$ for all $i \in [d]$, and a, b are hyperparameters. Note that given μ, ρ, ξ and τ^2, we can write the model in autoregressive form as

$$\boldsymbol{X}_t = \boldsymbol{\mu} + \rho(\boldsymbol{X}_{t-1} - \boldsymbol{\mu}) + \boldsymbol{v}_t \tag{C.1}$$

where $\boldsymbol{\mu} = \mu\mathbf{1}$, $\mathbf{1}$ is the d-dimensional vector of ones, i.e., $\mathbf{1} = (1, \ldots, 1) \in \mathbb{R}^d$, and

$$v_{i,t} = u_{i,t} + \nu_{i,t} - u_{i,t-1},$$

where $\boldsymbol{\nu}_t \sim \mathrm{N}(\mathbf{0}, \tau^2\mathbf{Q}^{-1})$ are spatially correlated effects on the mean. Note that

$$\boldsymbol{v}_t \sim \mathrm{N}\{0, (\tau^2\mathbf{Q}^{-1} + 2\sigma_u^2\mathbf{I_d})\},$$

thus,

$$\tilde{\boldsymbol{v}}_t = \mathbf{C}^{1/2}\boldsymbol{v}_t \sim \mathrm{N}\{\mathbf{0}, \mathbf{I_d}\},$$

where $\mathbf{C} = (\tau^2\mathbf{Q}^{-1} + 2\sigma_u^2\mathbf{I_d})^{-1}$ is the covariance matrix.

C.2 GNAR model

The global-α GNAR$(p, [s_k])$ is given by

$$
\begin{aligned}
\boldsymbol{Z}_{r,t} &= (\mathbf{S}_r \odot \mathbf{W})\boldsymbol{X}_t \\
\boldsymbol{X}_t &= \sum_{k=1}^{p}\left(\alpha_k\boldsymbol{X}_{t-k} + \sum_{r=1}^{s_k}\beta_{kr}\boldsymbol{Z}_{r,t-k}\right) + \boldsymbol{u}_t,
\end{aligned} \tag{C.2}
$$

where $\boldsymbol{u}_t \sim \mathrm{N}_d(0, \mathbf{\Sigma_u})$, s_k is the maximum r-stage depth at lag k (i.e., the number of nonzero β_{kr} parameters at lag k), and p is the maximum lag.

C.3 CAR as a GNAR model

Notice that by constraining (C.2) to no neighbourhood regressions and one-lag, i.e, model order $(1, [0])$, we can estimate the spatial random effects by generalised least-squares by setting the covariance matrix equivalence $\boldsymbol{\Sigma}_{\mathbf{u}} = (\tau^2\mathbf{Q}^{-1} + 2\sigma_u^2\mathbf{I}_{\mathbf{d}})^{-1}$, and by including an intercept term $\boldsymbol{\mu}$, we can write (C.2) as

$$\boldsymbol{X}_t = \boldsymbol{\mu} + \alpha_1(\boldsymbol{X}_{t-1} - \boldsymbol{\mu}) + \boldsymbol{v}_t,$$

where $\boldsymbol{v}_t \sim \mathrm{N}(0, \boldsymbol{\Sigma}_{\mathbf{u}})$, which is identical to the CAR model given by (C.1).

Further, note that by the partitioned matrix inverse formula we have that

$$[\mathbf{Q}]_{i\cdot} = -\mathbf{Q}_{-i}[\mathbf{Q}^{-1}]_{i\cdot},$$

thus, non-zero entries correspond to 1-stage neighbours. Let $w_{i\cdot} = [\mathbf{Q}]_{i\cdot}$, i.e., the ith row of $\mathbf{Q}$ without the diagonal entry. Then, by properties of the multivariate normal distribution, given all other random effects, i.e., $\phi_{j,t}$ for $j \neq i$, we can write

$$\phi_{i,t} = \rho\phi_{i,t-1} + \beta\sum_{j=1}^{d} q_{ij}(\phi_{j,t} - \rho\phi_{j,t-1}) + u_{i,t},$$

where $\beta = \xi(\tau^2 + \sigma_u^2)^{-1}$. Notice that if we set $\boldsymbol{\varphi}_t = \{\mathbf{Q} - \mathrm{diag}(\mathbf{Q})\}\boldsymbol{\phi}_t$, then we have that

$$\boldsymbol{\phi}_t = \rho\boldsymbol{\phi}_{t-1} + \beta(\boldsymbol{\varphi}_t - \rho\boldsymbol{\varphi}_{t-1}) + \boldsymbol{u}_t,$$

which should be thought as conditional given all other entries for each random effect $\phi_{i,t}$. This is a global-α GNAR process, albeit, using conditional distributions for 1-stage neighbourhood regressions, which might result in unstable estimators. The non-normalised weights matrix is $\{\mathbf{Q} - \mathrm{diag}(\mathbf{Q})\}$.

C.4 One-step forecast

Assume that we observe a realisation of length T. Then, we estimate the unknown parameters in (C.1) by Markov Chain Monte Carlo and compute one-step forecasts by inputting $\hat{\boldsymbol{\mu}}$ and $\hat{\rho}$, i.e,

$$\hat{\boldsymbol{X}}_{T+1} = \hat{\boldsymbol{\mu}} + \hat{\rho}(\boldsymbol{X}_T - \hat{\boldsymbol{\mu}}),$$

note that we can also compute the above for each set of parameters sampled from the posterior, and subsequently compute the predictive one-step forecast, which integrates the parameters. However, computation is cumbersome and we could not find a forecast option in `CARBayesST`.

Alternatively, the *generalised least squares* estimator is given by

$$\hat{\boldsymbol{\theta}} = (\mathbf{R}^T\boldsymbol{\Sigma}_T^{-1}\mathbf{R})^{-1}\mathbf{R}^T\boldsymbol{\Sigma}_T^{-1}\boldsymbol{y}_T,$$

where we have written a length T realisation in linear model form, i.e., $\boldsymbol{y}_T = \mathbf{R}\,\boldsymbol{\theta} + \boldsymbol{u}_T$, $\boldsymbol{u}_T \sim \mathrm{N}(0, \boldsymbol{\Sigma}_T)$, $\boldsymbol{\Sigma}_T = \mathbf{I}_{\mathbf{d}} \otimes \boldsymbol{\Sigma}_{\mathbf{u}}$, and $\boldsymbol{\theta} = (\mu, \rho) \in \mathbb{R}^2$ is the vector of unknown autoregressive parameters. The one-step forecast is given by

$$\hat{\boldsymbol{X}}_{T+1} = \hat{\boldsymbol{\theta}}_1 + \hat{\theta}_2(\boldsymbol{X}_T - \hat{\boldsymbol{\theta}}_1),$$

where $\hat{\boldsymbol{\theta}}_1 = \hat{\theta}_1 \mathbf{1}$. Notice that it strongly resembles the one computed using Markov Chain Monte Carlo. Further, if we assume that $\boldsymbol{X}_t$ is a global-α GNAR$(1, [0])$ process with spatial (network informed) correlated errors, then the estimator is

$$\hat{\boldsymbol{\theta}} = (\mathbf{R}^T \boldsymbol{\Sigma}_T^{-1} \mathbf{R})^{-1} \mathbf{R}^T \boldsymbol{\Sigma}_T^{-1} \boldsymbol{y}_T,$$

which is identical to the generalised least squares estimator for CARar models. Thus, one-step ahead forecasts computed by inputting $\hat{\boldsymbol{\theta}}$ are equal for GNAR$(1, [0])$ with correlated errors and CARar(1) models.

C.5 Some CARar limitations

- CARar is difficult to extend, e.g. adding a functional mean or penalty term, which would be easy for GNAR.
- **Forecasting difficulty:** No clear n-step ahead forecast computation, not even for $n = 1$. There appears to be no general method for forecasting hierarchical models in a fully Bayesian way; see Chapter 7 in Gelman et al. (2013).
- Difficult to compare/mix multiple CAR models (e.g. with GNAR we can imagine multiple networks for the same vector time series and then do bagging).
- Random effects in CARar are perhaps difficult to interpret.
- Constrained to one-stage neighbours (in current formulations).
- Software limited to lag-two models (might not capture higher lag seasonality).

C.6 Conclusion

Interestingly, we can think of CAR models as computationally expensive overparameterized GNAR models constrained to one-stage neighbourhood regressions. Thus, these models cannot capture higher-order interactions, further, forecasting and comparing multiple models is cumbersome. However, they provide a straightforward option for integrating spatial autocorrelation into GNAR. By parameterizing the error covariance accordingly with $\mathbf{Q}$, and performing estimation in alternating fashion via generalised least squares.

D Global node relevance

We propose a diagnostic statistic for quantifying the relevance each node has on the network time series correlation structure. After selecting model order $(\hat{p}, [\hat{s_k}])$ based on some data-dependent criterion, e.g., quick visual inspection of Corbit plots, we can find the largest active r-stage order term $\hat{r} := \max\{[\hat{s_k}]\}$, which estimates r^*. Using the data-dependent $\hat{r}$, we compute the active weights matrix, i.e., $\mathbf{W}$ constrained to nodes at a maximum distance of $\hat{r}$ (no path is longer between active nodes), this matrix is $\mathbf{W} \odot \mathbf{S}_{(\hat{r})}$, where

$\mathbf{S}_{(\hat{r})} = \sum_{\ell=1}^{\hat{r}} \mathbf{S}_\ell$. Combining model order selection and the resulting autocovariance bound, as given in Definition 3, motivates the global relevance index given below

$$\text{globindex}(X_{i,t}|\,\hat{r}) := \left(\sum_{j=1}^{d}[\mathbf{W} \odot \mathbf{S}_{(\hat{r})}]_{ji}\right)\left\{\max_{l\in\mathcal{K}}\left(\sum_{j=1}^{d}[\mathbf{W} \odot \mathbf{S}_{(\hat{r})}]_{jl}\right)\right\}^{-1},$$

which computes the ratio between the largest column sum for active nodes and a particular node. We interpret this as the relevance each node has globally on the correlation structure. By (17), this node upper bounds the covariance structure in the sense that removing it would change the autocovariance bound, the resulting (P)NACF values and possibly our choice of model.

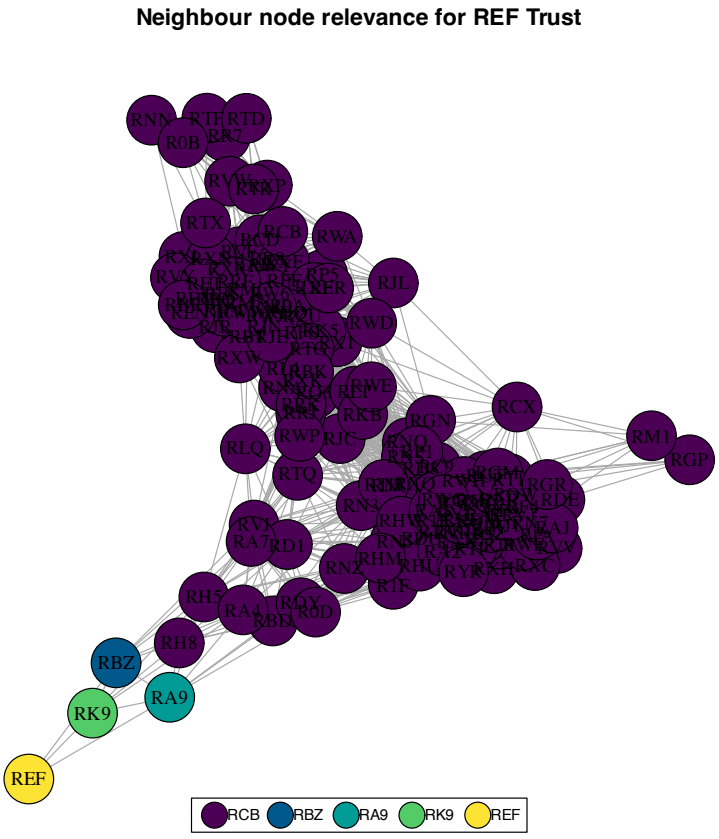

Figure 11: Neighbouring node relevance for Trust REF imposed on the network. Values are from zero to one, and equal one for the local node, i.e., REF. See Section 5.4 for a more detailed discussion.

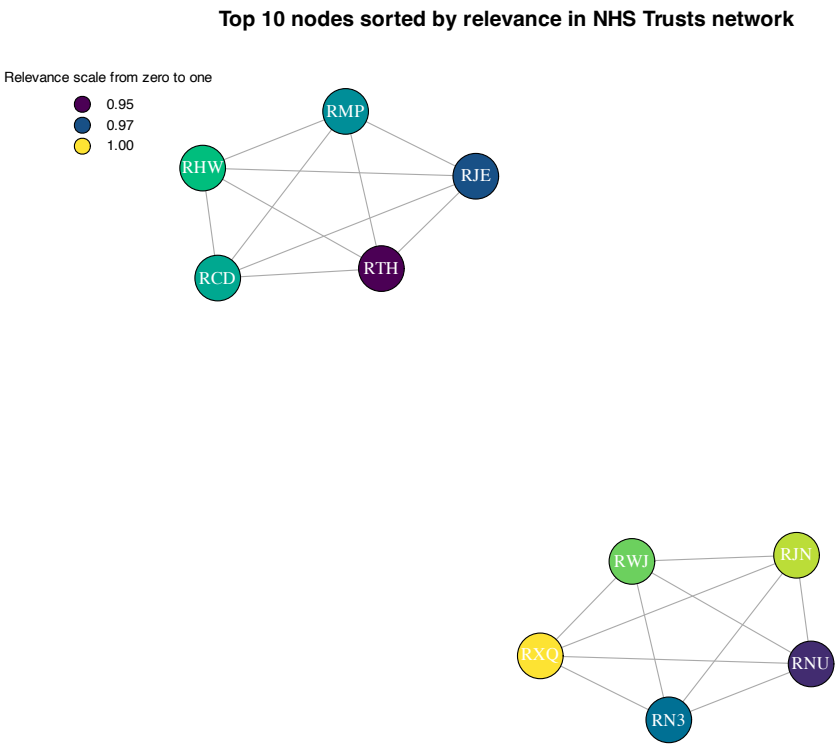

Figure 12: Top 10 relevant nodes as given by (18) for $r^* = 1$. The two clusters are well separated between the south and north of England.

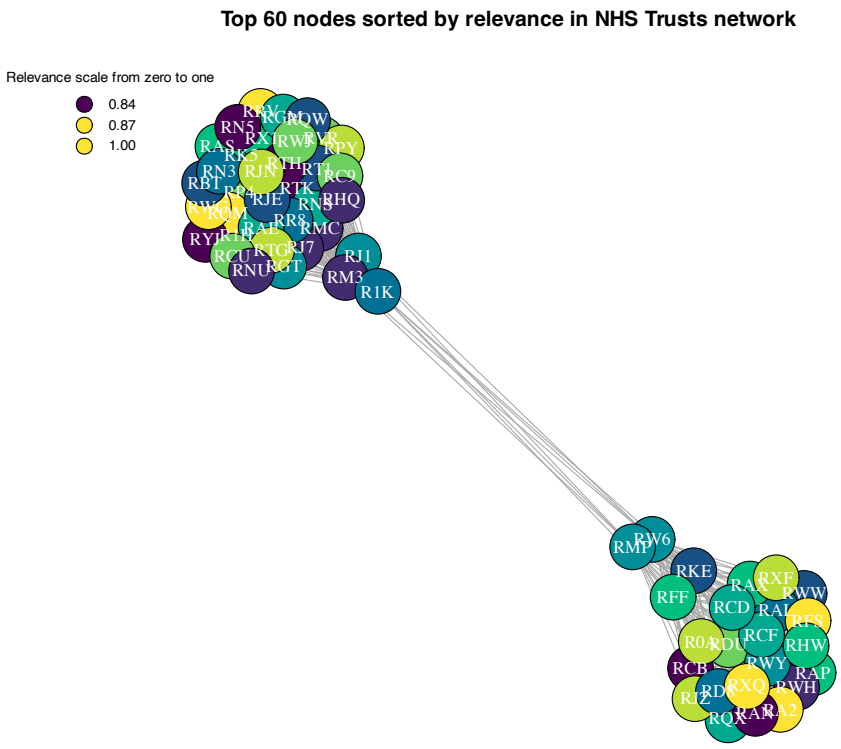

Figure 13: Top 60 relevant nodes as given by (18) for $r^* = 1$. The two clusters in Figure 12 are now connected. Further, points not previously between relevant nodes in the north are now present. Interestingly, the previous most relevant nodes in the south are the ones that connect London to Bristol and Southampton, i.e., new relevant nodes are concentrated near London.

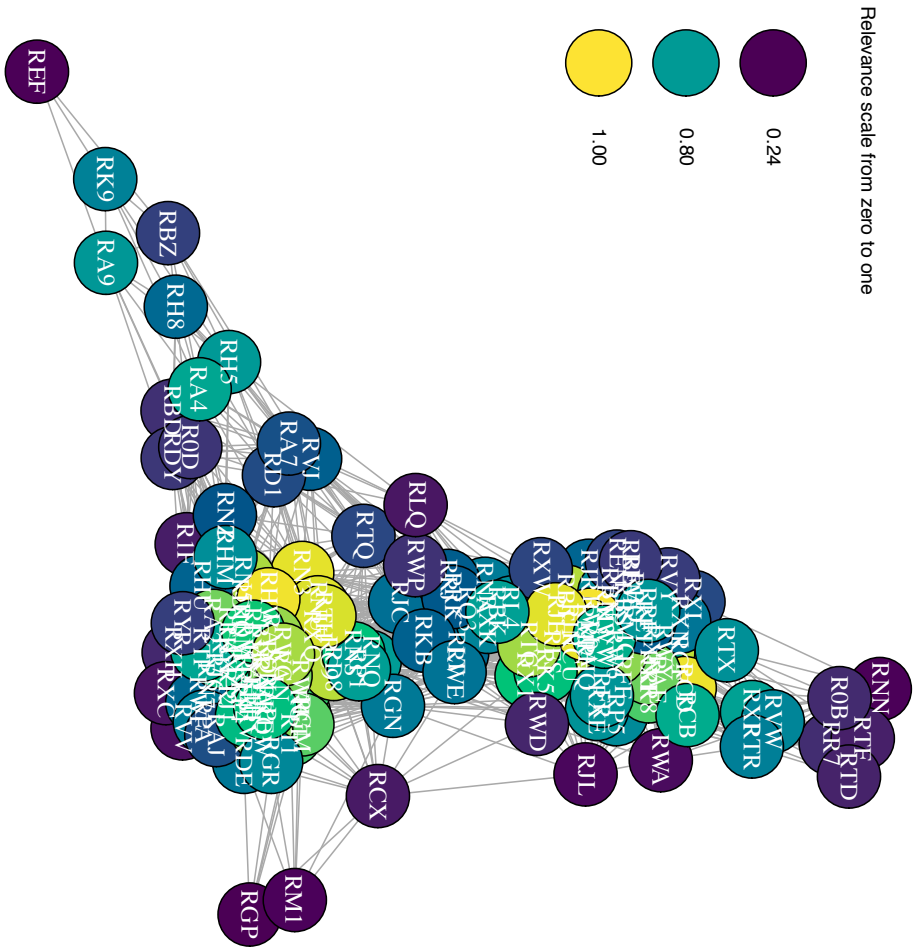

Figure 14: Node relevance hierarchy imposed on the network.

References

Akaike, H. (1973) Information theory and an extension of the maximum likelihood principle, in *Proceedings of the 2nd International Symposium on Information Theory*, pp. 267–281, Academiai Kiado, Budapest Hungary.

Armillotta, M. and Fokianos, K. (2021) Poisson network autoregression, arXiv:2104.06296.

Armillotta, M. and Fokianos, K. (2024) Count network autoregression, *Journal of Time Series Analysis*, **45**, 584–612.

Brillinger, D. R. (1981) *Time Series: Data Analysis and Theory*, Holt, Rinehart and Winston, New York.

Brockwell, P. J. and Davis, R. A. (2006) *Time Series: Theory and Methods*, Springer-Verlag, New York, 2nd edition.

Butts, C. T. (2023) *sna: Tools for Social Network Analysis*, R package version 2.7-1.

Chatfield, C. (2004) *The Analysis of Time Series: An introduction*, Chapman and Hall/CRC Press, Boca Raton.

Csardi, G. and Nepusz, T. (2006) The igraph software package for complex network research, *Complex Systems*, **1695**, 1–9.

Dahlhaus, R. (2000) Graphical interaction models for multivariate time series, *Metrika*, **51**, 157–172.

Dallakyan, A., Kim, R., and Pourahmadi, M. (2022) Time series graphical lasso and sparse VAR estimation, *Comp. Stat. Data Anal.*, **176**, 107557.

DEFRA (2011) Foot and mouth control strategy for Great Britain, Department for Environment and Rural Affairs, The Scottish Government, and The Welsh Government, (https://www.gov.uk/government/publications/foot-and-mouth-disease-control-strategy-for-great-britain).

Dijkstra, E. W. (1959) A note on two problems in connexion with graphs, *Numer. Math.*, **1**, 269–271.

Epskamp, S. and Fried, E. I. (2018) A tutorial on regularized partial correlation networks, *Psychol. Methods*, **23**, 617–634.

Friedman, J., Hastie, T., and Tibshirani, R. (2008) Sparse inverse covariance estimation with the graphical lasso, *Biostatistics*, **9**, 432–441.

García Rasines, D. and Young, G. (2023) Splitting strategies for post-selection inference, *Biometrika*, **110**, 597–614.

Garnier, S., Ross, N., Rudis, B., Sciaini, M., Pedro Camargo, A., and Scherer, C. (2023) *viridis - Colorblind-Friendly Color Maps for R*, R package version 0.6.4.

Gelman, A., Carlin, J. B., Stern, H. S., Dunson, D. B., Vehtari, A., and Rubin, D. B. (2013) *Bayesian Data Analysis*, Chapman & Hall/CRC Texts in Statistical Science Series, CRC, Boca Raton, Florida, third edition.

Hastie, T., Tibshirani, R., and Friedman, J. (2017) *The Elements of Statistical Learning*, Springer, New York, 2nd edition.

Haydon, D. T., Kao, R. R., and Kitching, R. P. (2004) The UK foot-and-mouth disease outbreak — the aftermath, *Nat. Rev. Microbiol.*, **2**, 675–681.

Hyndman, R. J. and Khandakar, Y. (2008) Automatic time series forecasting: the forecast package for R, *J. Statist. Soft.*, **26**, 1–22.

Hyndman, R. J., Athanasopoulos, G., Bergmeir, C., Caceres, G., Chhay, L., O'Hara-Wild, M., Petropoulos, F., Razbash, S., Wang, E., and Yasmeen, F. (2023) *forecast: Forecasting functions for time series and linear models*, R package version 8.21.

Kahle, D. and Wickham, H. (2013) ggmap: Spatial visualization with ggplot2, *The R Journal*, **5**, 144–161.

Knight, M., Nason, G., and Nunes, M. (2016) Modelling, detrending and decorrelation of network time series, arXiv:1603.03221.

Knight, M., Leeming, K., Nason, G. P., and Nunes, M. (2020) Generalized network autoregressive processes and the GNAR package, *J. Statist. Soft.*, **96**, 1–36.

Knight, M., Leeming, K., Nason, G. P., and Nunes, M. (2023) *GNAR: Methods for Fitting Network Time Series Models.*, R package version 1.1.1.

Kolaczyk, E. (2009) *Statistical Analysis of Network Data: Methods and Models*, Springer-Verlag, New York.

Lauritzen, S. L. (2004) *Graphical Models*, Oxford University Press, Oxford.

Lee, D., Rushworth, A., and Napier, G. (2018) Spatio-temporal areal unit modeling in R with conditional autoregressive priors using the CARBayesST package, *J. Statist. Soft.*, **84**, 1–39.

Leeming, K. (2019) *New methods in time series analysis*, Ph.D. thesis, University of Bristol, Bristol, UK.

Liu, S., Chen, L., Dong, H., Wang, Z., Wu, D., and Huang, Z. (2019) Higher-order weighted graph convolutional networks, arXiv:1911.04129.

Lütkepohl, H. (2005) *New Introduction to Multiple Time Series Analysis*, Springer-Verlag, Berlin.

Mantziou, A., Cucuringu, M., Meirinhos, V., and Reinert, G. (2023) The GNAR-edge model: a network autoregressive model for networks with time-varying edge weights, *J. Complex Netw.*, **11**, cnad039.

Mathieu, E., Ritchie, R., Rodés-Guirao, L., Appel, C., Giattino, C., Hasell, J., Macdonald, B., Dattani, S., Beltekian, D., Ortiz-Ospina, E., and Roser, M. (2022) Coronavirus pandemic (COVID-19), https://ourworldindata.org/coronavirus (accessed September 9th, 2024).

Nason, G. and Wei, J. (2022) Quantifying the economic response to COVID-19 mitigations and death rates via forecasting purchasing managers' indices using generalised network autoregressive models with exogenous variables (with discussion), *J. R. Statist. Soc. A*, **185**, 1778–1792.

Nunes, M., Knight, M., and Nason, G. (2015) Modelling and prediction of time series arising on a graph, in A. Antoniadis, J.-M. Poggi, and X. Brossat, eds., *Modeling and Stochastic Learning for Forecasting in High Dimensions*, volume 217 of *Lecture Notes in Statistics*, pp. 183–192, Springer-Verlag, New York.

Pfaff, B. (2008a) *Analysis of Integrated and Cointegrated Time Series with R*, Springer, New York, 2nd edition.

Pfaff, B. (2008b) VAR, SVAR and SVEC models: Implementation within R package vars, *J. Statist. Soft.*, **27**.

Pfaff, B. (2023) *vars: VAR, SVAR and SVEC Models*, R package version 1.5.9.

R Core Team (2022) *R: A Language and Environment for Statistical Computing*, R Foundation for Statistical Computing, Vienna, Austria, version R 4.3.2.

Rushworth, A., Lee, D., and Mitchell, R. (2014) A spatio-temporal model for estimating the long-term effects of air pollution on respiratory hospital admissions in greater london, *Spatial and Spatio-temporal Epidemiology*, **10**, 29–38.

Schwarz, G. (1978) Estimating the dimension of a model, *Ann. Statist.*, **6**, 461–464.

Shumway, R. H. (2017) *Time Series Analysis and Its Applications With R Examples*, Springer, New York, 4th edition.

Silva, V. F., Silva, M. E., Ribeiro, P., and Silva, F. (2021) Time series analysis via network science: Concepts and algorithms, *WIREs Data Mining and Knowledge Discovery*, **11**, e1404.

Songsiri, J., Dahl, J., and Vandenberghe, L. (2009) Graphical models of autoregressive processes, in D. Palomar and Y. C. Eldar, eds., *Convex Optimization in Signal Processing and Communications*, pp. 89–116, Elsevier.

Vazzoler, S. (2021) *sparsevar: Sparse VAR/VECM Models Estimation*, R package version 0.1.0.

Wainwright, M. J. (2019) *High-Dimensional Statistics: A Non-Asymptotic Viewpoint*, Cambridge University Press, Cambridge.

Wickham, H. (2016) *ggplot2: Elegant Graphics for Data Analysis*, Springer-Verlag, New York.

Wu, F., Souza, A., Zhang, T., Fifty, C., Yu, T., and Weinberger, K. (2019) Simplifying graph convolutional networks, in K. Chaudhuri and R. Salakhutdinov, eds., *Proceedings of the 36th International Conference on Machine Learning*, volume 97 of *Proceedings of Machine Learning Research*, pp. 6861–6871, PMLR.

Yin, H., Safikhani, A., and Michailidis, G. (2023) A general modeling framework for network autoregressive processes, *Technometrics*, **65**, 579–589.

Zhou, J., Li, R., Pan, R., and Wang, H. (2020) Network GARCH model, *Statist. Sci.*, **30**, 1–18.

Zhu, X., Pan, R., Li, G., Liu, Y., and Wang, H. (2017) Network vector autoregression, *Ann. Statist.*, **45**, 1096–1123.

Zhu, X., Wang, W., Wang, H., and Härdle, W. (2019) Network quantile autoregression, *J. Econometrics*, **212**, 345–358.